Microfluidic-based Fluorescence Detection for Biomarker Analysis

Shihan Xu

A dissertation

submitted in partial fulfillment of the

requirements for the degree of

Doctor of Philosophy

University of Washington

2022

Reading Committee:

Daniel T. Chiu, Chair

Patrick S. Stayton

Bo Zhang

Program Authorized to Offer Degree:

Bioengineering

University of Washington

Abstract

Microfluidic-based Fluorescence Detection for Biomarker Analysis

Shihan Xu

Chair of the Supervisory Committee:

Professor Daniel T. Chiu

Bioengineering, Chemistry

In this dissertation, 2 platforms are described with the combination of microfluidics and fluorescence detection for biomarker analysis. The first platform described here is to isolate CTCs with high purity by using 2-stage sorting technique and herringbone features for aliquot stretching, including axial and lateral mixing to spread cells. We achieved a roughly 70-fold improvement in target cell purity to 70%, compared to our previous 1-stage eDAR platform with 1% purity. With the 8.8cm channel and herringbone features, Single CTCs can be collected with less than one contaminating WBC, making sequential eDAR (S-eDAR) amenable to downstream analyses such as single-cell sequencing and single-cell fluorescence in situ hybridization (FISH). S-eDAR was further applied to recover rare cells from concentrated PBMCs at a recovery rate of over 85%, similar to the performance of S-eDAR

when using whole blood samples. However, by using concentrated PBMCs, the required sample volume was reduced, and the antibody cost was reduced by 20-fold. We applied S-eDAR to sort rare fetal nucleated red blood cells (fNRBCs) from cord blood and adult female PBMCs into which cord blood cells were added, demonstrating the potential of S-eDAR for isolating fNRBCs from maternal blood for noninvasive prenatal diagnosis. At the end, fNRBCs were successfully enriched from 2nd trimester blood and confirmed with immunostaining.

To complement CTCs analysis, the single-molecule sensitive flow platform was applied to enable surface protein profiling on exosomes. The platform was validated with single molecules first, including alexa647 anti-IgG and PE anti-IgG. The recovery rate for these 2 molecules were higher than 90%, indicating the high sensitivity of detecting single molecules with this platform. After validation, DiFi EVs (from DiFi human colorectal cancer cell line) were labeled with a membrane dye (Anepps) and Phycoerythrin (PE)-tagged antibodies (3 common tetraspanin markers, including CD9, CD63 and CD81 and epidermal growth factor receptor (EGFR)). Based the colocalization of fluorescence signals from protein markers and membrane dye, antibody-labeled exosomes can be clearly differentiated from free antibodies. This platform can characterize surface proteins on exosomes and analyze their heterogeneity as a potential complement analysis for CTCs. Furthermore, this platform can characterize EV subpopulations with multiplex protein labeling, which is useful for early detection of cancers and characterize the dynamic change of tumors at different stages and their heterogeneity.

Acknowledgements

Curiosity is the key to open the door to science. I know this from my advisor, Dr. Daniel T. Chiu. I wouldn't finish my PhD program without his guidance, support and questioning. His scientific thinking, rigorous and diligent working altitude encourage me all the time. What I've learned from Dr. Chiu will benefit me forever.

I would also like to thank my committee, Dr. Patrick Stayton, Dr. Linda Shapiro and Dr. Bo Zhang, for their guidance. I appreciate the advises they gave me and their support during this learning journey.

I am grateful for the collaboration with Dr. Hilary Gammill, MD, Dr. Lucia Vojtech, Dr. Michael Gravett, MD. I want to thank all patients who were willing to donate their blood and make their contribution for scientific research. Next, I want to thank all my colleagues for collaborations and help in these years, especially I want to thank Li Wu, Yifei, James, Seung Ryoung, Yuling, Eleanor, Mengxia and Yuanhua. I also want to thank Perry and Hui-Min from MiCareo for the collaboration on the sequential eDAR projects.

I am so lucky to meet many friends in Seattle. I appreciate the time spending with you guys, and all things I learned from you guys. I want to thank Jingyi, Ana, Emily, Yue, Lingling, Tiffany, Ze, Kan and Zhongwei. Thank Teng, Xiaowu and Axin for the care and support from thousands of miles away.

At last, I want to thank my family, my parents and grandparents. Their unconditional supports and attitude in life encourage me to learn more, think more and never give up.

Table of Contents

List of Figures

List of Tables

Chapter 1 Introduction

Cancer was the second leading cause of death in the United States. In 2020, there were around 600,000 cancer deaths. Most cancer deaths are due to cancer metastasis. Cancer often metastasizes to other parts of the body, such as the brain, liver and bones. At the beginning of cancer metastasis diagnosis, various imaging tests can be applied for screening on different organs, including X-ray, Magnetic resonance imaging (MRI), Computed tomography (CT). For actual diagnosis, tissue biopsy was made by using hollow needles to get cells from a suspicious area and looking at cells in the lab. This tissue biopsy has high invasiveness, high cost, and is limited for localized cancer. For monitoring of cancer development, re-biopsy is often needed.

Instead of invasive tissue biopsy, liquid biopsy is gaining more focus in recent years. With the introduction of novel techniques on liquid biopsy, various aspects of cancer-related management including early detection of cancer metastasis, early diagnosis and screening, serial sampling and efficient longitudinal monitoring of disease progress and response to treatment were improved, especially for breast cancer.[1] With liquid biopsy, various biomarkers can be analyzed, including circulating rare cells, exosomes, cell-free DNA/RNA, etc. In this dissertation, I am focusing on two biomarkers, circulating rare cells, which includes circulating tumor cells (CTCs) and fetal nucleated red blood cells (fNRBCs), and exosomes, which can provide significance for the early detection of various diseases.

1.1 Circulating Tumor Cells and Isolating Techniques

Most cancer deaths are due to tumor metastasis. Before cancer metastasizes, cancer cells are disseminated from the primary tumor site to remote sites through blood circulation.[2] CTCs have been detected in many epithelial cancers, including breast, prostate, lung, and colon. Both patients with metastatic lesions and localized cancers are reported to have CTCs detected in their blood.[3] These CTCs are precursors to cancer metastasis. CTC count analysis from peripheral blood can be used to determine prognosis of cancer. An arbitrary cutoff value (5 circulating tumor cells per 7.5 mL of blood) was chosen to distinguish patients with an unfavorable prognosis from patients with a favorable prognosis.[4] Potentially, CTCs could be used as a marker for disease progression and survival in real time.

Furthermore, analyses of CTCs at the single-cell resolution in peripheral blood could offer a minimally invasive approach to characterize dynamic changes in tumor heterogeneity in individual patients with cancer at the genomic, transcriptomic, proteomic and functional levels.[5] CTCs have the potential to allow longitudinal monitoring of patients about therapy effectiveness, guide therapeutic management, detect cancer metastases which are not detectable by other methods, and offer insights into mechanisms of drug resistance.[6] However, due to a lack of robust platforms or technologies to enrich sufficient numbers of CTCs to analyze gene mutations and CTC heterogeneity, lots of CTC genomics remain undiscovered.[7]

In recent years, advances in CTC isolation has been developed widely for the use of CTCs as a real-time liquid biopsy.[8] However, owing to their low abundance (tens to hundreds per ml

of whole blood)[9-11] and heterogeneity,[12] detection and isolation is difficult. A variety of approaches to isolate CTCs have been developed, falling into two main categories: physical isolation and biomarker/antibody-based methods.[13] Physical isolation methods are based on differences in the cell size, density or other physical characteristics. For example, CTCs are typically larger than blood cells and can be isolated by filtration[14-18] or flow fractionation.[19] Filtration is fast and simple but the size overlap between CTCs and white blood cells (WBCs)[20] might cause low purity. Differential flow patterns of cells in microfluidic channels have been used to isolate CTCs from blood cells.[21] Dielectrophoretic detection methods[22] based on structural differences between CTCs and WBCs (including size) were developed to achieve high purity.

Antibody-based methods include: (1) Immunomagnetic isolation that a magnetic field is applied to separate antibody-bound CTCs/epithelial cells.[23-25] CellSearch®, the main FDA-approved CTC detection platform, employs immunomagnetic isolation.[26] (2) Surface capture with microfluidics: CTCs are captured by antibodies immobilized on the surface of a microfluidic chip,[27-30] and advanced microfluidic flow patterns can be added to improve the outcome.[31, 32] (3) Fluorescent antibody labeling: CTCs labeled by fluorescent anti-CTC antibodies are detected using laser-induced fluorescence with high sensitivity.[33] Two concerns on antibody-based method, especially for fluorescent antibody labeling on CTCs: (1) low expression level of protein markers or heterogeneity of CTCs and (2) false positive cells.

Epithelial cell adhesion molecule (EpCAM) is most used to enrich circulating tumor cells

because its popular expression in cells of epithelial origin, even in variable expression level (heterogeneity), and it is absent in blood cells. However, during the epithelial-to -mesenchymal transition, different subsets of CTCs can show a range of phenotypes. If the expression level of antibody markers is low, causing the fluorescent intensity of labeled CTCs to be lower than the detection limit of system and not to be detected. Thus, the use of specific cocktails of cell surface epithelial and mesenchymal markers is necessary to enrich all subsets of CTCs.[34] However, individual blood cells might also be labeled by at least one of these cocktail markers, which would lead to false-positive results. For an unambiguous detection of CTCs, except phenotyping by immunostaining, additional genomic analyses are complemented to avoid false-positive findings including PCR, fluorescence in situ hybridization (FISH) and single cell sequencing.[13]

1.2 The eDAR Platform and Applications

Microfluidics is a system that can process small quantities of fluids by using microscale channels, typically 10-100 μm. It has so many advantages, including high sensitivity and throughput, multiplexed and highly paralleled assays, faster analyses, low reagent consumptions, low cost, integrated and simplified process, allowing microfluidics popularly used in many applications, such as separation, DNA analysis and immunoassay, chemical synthesis and enzymatic reactions.

In 2012, our group developed an ensemble decision aliquot ranking (eDAR) platform combining microfluidics and fluorescence detection with a line-confocal design for isolating

CTCs from whole blood (Figure 1.1). The rare-cell isolation platform consists of an optical detection system, a microfluidic active sorting scheme, and a cell capture chamber for cell enumeration. The optical detection system uses laser-induced fluorescence detection across the width of a microfluidic channel.[35] The sorting scheme consists of a junction where upon detection, CTCs are diverted to a channel leading to on-chip filters. Trapped cells can be fixed, permeabilized, and labeled with antibodies prior to enumeration in the chamber. The CTCs were readily detected in the 2 nL aliquots of blood with an average signal-to-noise (S/N) ratio of 32 for the EpCAM marker and 64 for the Her2 marker[36] and labeled cells in whole blood samples can be detected in multiple colors and enumerated from detection traces.[37] Compared to CellSearch, the FDA-approved platform to detect CTCs on clinical samples, which detected 0 to 64 CTCs with an average of 5, while eDAR recovered 11 to 105 CTCs with an average of 44 from same clinical samples, indicating the improved sensitivity offered by the eDAR.

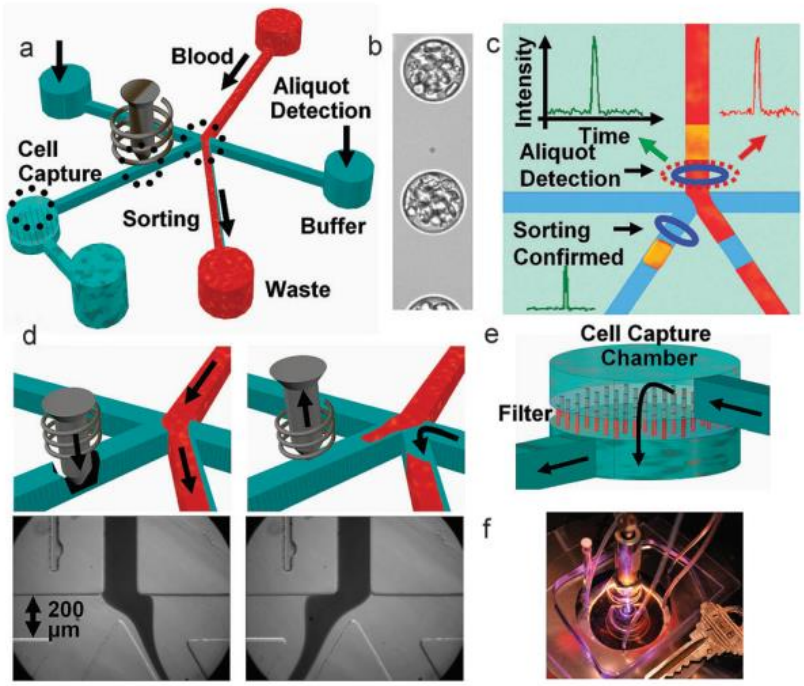

Figure 1.1 Schematic and images showing how eDAR works. a) Overview of the microfluidic chip. b) A high-speed camera image of whole blood aliquoted into a continuous stream of droplets c) Aliquot detection: laser-induced fluorescence triggers the sorting of an aliquot containing a rare cell (shown in yellow) to the collection microchannel and cell capture chamber. d) Sorting: The solenoid piston is released to allow flow through the collection channel; images at the bottom show the flow of whole blood when the collection channel is closed (left) and opened (right). e) Cell capture: The collected aliquots are filtered through a membrane to remove blood cells from the target cells and leave the captured cells isolated and accessible for further study. f) Photograph of an eDAR chip.[36]

In Figure 1.2, the next generation of eDAR was designed and optimized with a new hydrodynamic switching scheme for the active sorting step in eDAR, which provided fast cell sorting with an improved reproducibility and stability.[35] The microfluidic chip was further simplified by incorporating a functional area for subsequent purification using micro-slits fabricated by a standard lithography method. This platform can be readily applied to enrich many types of rare cells with positive markers, including circulating fetal cells for non-invasive prenatal diagnosis, rare functional T cells for immune diseases.

For this platform, there are 2 drawbacks need to be improved. The first one is releasing cells from filters for downstream analysis is hard and the second one is the purity is too low (1%), not enabling convenient downstream analysis, such as single cell sequencing. To overcome these two problems, my projects focus on developing new generation of the platform without using any size-based filters to retain target cells, but achieving high purity of circulating rare cells with novel microfluidic designs, which enable convenient molecular characterization with single-cell sequencing, FISH, etc. Furthermore, the new platform can be applied on enriching other types of circulating rare cells in whole blood with specific antibody markers (e.g., circulating fetal nucleated red blood cells, circulating trophoblasts).

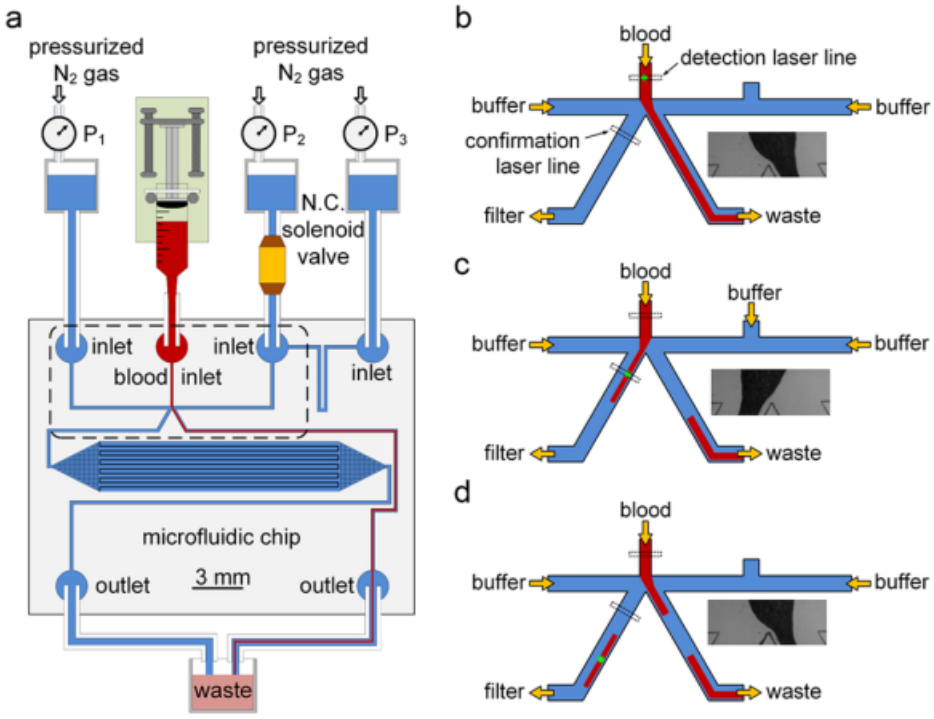

Figure 1.2 Microfluidic chip and hydrodynamic switching scheme of eDAR. (a) General structure of the microfluidic chip and the configuration of the eDAR platform. The bottom left channel was to collect sorted aliquots and transfer them to the subsequent purification area, which had 20 000 microslits. The area marked with a dashed box is further explained in (b)-(d). (b) The flow condition when no positive aliquot was ranked. (c) The blood flow was switched to the CTC collection channel, and the sorted aliquot was confirmed by the second APD. (d) The blood flow was switched back after the aliquot was sorted.[35]

Reprinted with permission from Zhao, Mengxia, et al. "New generation of ensemble-decision aliquot ranking based on simplified microfluidic components for large-capacity trapping of circulating tumor cells." Analytical chemistry 85.20 (2013): 9671-9677. Copyright 2013 American Chemical Society.

1.3 Fetal Nucleated Red Blood Cells

Noninvasive prenatal diagnosis is becoming increasingly common with advances in technologies for isolating DNA and fetal cells from maternal peripheral blood. Cell-free fetal DNA (cffDNA) purified from maternal blood can be used to detect trisomy and other genetic disorders, but is fragmented and surrounded by excess maternal DNA, and cannot be used to detect gene translocation or deletion. Although prospective studies have shown excellent performance of cffDNA based noninvasive prenatal screening for trisomy 21, 18, and 13, and the aid in the diagnosis of other pregnancy disorders, including preeclampsia, fetal growth restriction, stillbirth and detection of aneuploidy, the positive predictive value remains limited, and follow up diagnostic testing remains essential.

Compared with cffDNA, circulating fetal cells are advantageous regarding to the whole genome analysis for noninvasive prenatal diagnosis because they contain the entire fetal genome, uncontaminated with maternal DNA.[38] Fetal cell types present in maternal blood during pregnancy include myeloid fetal progenitor cells,[39] fetal lymphocytes, syncytiotrophoblasts, fetal nucleated red blood cells (fNRBCs), and circulating extravillous trophoblasts (CTBs),[40, 41, 42] Of these, fetal lymphocytes and myeloid fetal progenitor cells are poor candidates for prenatal diagnosis because they persist in maternal blood for years after pregnancies, causing contamination from previous pregnancies[43] (male fetal progenitor cells can persist for as long as 27 years[39]). Syncytiotrophoblasts-large, multinucleated placental epithelial cells shed into maternal circulation during the first trimester, are also poor

candidates for prenatal diagnosis as they are trapped in lung capillaries and removed from circulation.[44] Invading extravillous trophoblasts (EVTs), which originate from endovascular trophoblasts in the lumen of spiral arteries and become CTBs after entering the maternal peripheral blood,[44] play key roles during pregnancy including placental anchoring, remodeling uterine spiral arteries, and preventing maternal immune attack on the placenta. Failure of these processes causes miscarriage, preterm birth, and preeclampsia.[45, 46] CTBs are a promising target for early fetal diagnosis because their short lifespan precludes contamination from previous pregnancies; however, they are extremely rare and methods to enrich them lacked consistency and repeatability. Furthermore, confined placental mosaicism is an obstacle to interpret the results obtained by analyzing CTBs. Confined placental mosaicism occurs when cells from placenta indicates an abnormal number of chromosomes, but the fetus has a normal number of chromosomes, and this affects about 1-2% of pregnancies.

The fNRBCs are a promising cell type for noninvasive prenatal testing with short life span (25-35 day half-life in adult circulation) preventing contamination from previous pregnancies. fNRBCs are abundant in fetal blood early in gestation,[47, 48] but they are rare in maternal peripheral blood with a reported occurrence ranging from 3-26 cells per mL.[49-51] They have been successfully enriched from maternal blood by MACS,[52] FACS,[53] and microfluidics techniques.[54] FNRBCs have been applied to detect chromosome aneuploidy (trisomy 21, 18 and 13, Klinefelter's syndrome and XXX syndrome),[50, 54-56] ABO hemolytic disease,[57] and

microdeletion syndromes.[56, 58]

Even though fNRBCs has been well established by developing enrichment and confirmation methods, but some disadvantages still exist. For example, high contamination with MACS, low recovery rate with FACS and time-consuming on fabricating microfluidic chips or releasing step. A facile way to isolate and collect interested cells for downstream analysis is demanding. Because of the advantages of new generation of eDAR platform, including convenient cell collection with high purity, viability and sensitivity, its application was extended to enrich this type of circulating rare cells, fNRBCs, with molecular charaterization for non-invasive prenatal diagnosis.

1.4 Exosome Protein Profiling

Exosomes, a biomarker in a much smaller scale (40-160 nm), which originate from the endosomal system are present in biological fluids and are involved in multiple physiological and pathological processes,[59] including various cancers, pregnancy disorders, cardiovascular diseases, neurodegenerative diseases and immune responses. Compared with circulating rare cells, exosomes are much more abundant in biological fluids. They are now considered as an additional mechanism for intercellular communication, allowing cells to exchange proteins, lipids, DNA and RNA. Exosomes show potentials for cancer diagnostics since they transport molecular contents (proteins, DNA and RNA) of the cells from where they originate. Detection and molecular profiling of exosomes is still challenging and their purification process is usually time-consuming.[60]

Surface proteins on exosomes can carry information about their tissues of origin and many research works indicated expression levels of certain proteins from exosomes had prognostic value for cancer diseases. Conventional detection standards, such as western blot analysis and enzyme-linked immunosorbent assays (ELISA), require large amounts of sample and extensive post-labeling processes for detection.[61] Their sensitivity is a concern, and the heterogeneity of individual exosomes was lost in pooled samples. In recent years, novel technology has been developed to increase the sensitivity of molecular profiling of exosomes, including multielectrode spectroscopy,[62] nano-plasmonic sensors,[60] a proximity-dependent barcoding assay (PBA).[63] Furthermore, some works are focused on single EV analysis, including imaging[64] and dedicated flow cytometry.[65] With imaging, multiplex protein markers on individual exosomes can be analyzed with multicolor labeling with different fluorophore-tagged antibodies, but the copy number of each marker has not been described.

Flow cytometry was popularly applied for cell subpopulations characterization with high throughput. In recent years, dedicated flow cytometry was optimized to characterize the protein expression level of each marker on individual exosomes and their size information.[65] But the accuracy of this method on copy number and size measurement was not clear, since it doesn't have single molecule sensitivity and uses calibration curves from beads for the copy number of protein markers and size characterization. It potentially misses small-size exosomes and exosomes with low copy number of protein markers (e.g., <15).

1.5 Project Overview

This dissertation summarizes my research as a Ph.D. student in Dr. Daniel T. Chiu's lab. My projects focus on the development of analytical methods combining microfluidics and fluorescence detection for biomarker analysis, including circulating rare cells and exosomes, aiming at providing robust platforms to analyze such biomarkers. It can be divided into three parts, from chapter 2 to 4.

Chapter 2 focuses on the development of a sequential eDAR (S-eDAR) platform for CTC isolation with 2-stage sorting to achieve high purity of CTCs. The microfluidic chips have 2-stage sorting mechanism for axial dispersion and herringbone structures as the second layer for lateral mixing of an aliquot between two sorting junctions. The recovery rate and purity of CTCs were confirmed with fluorescence imaging and S-eDAR for 2 rounds. With S-eDAR, the purity was enhanced to 70%, with less than 1 WBC per CTC. The sequential eDAR had a recovery efficiency of over 90% for cultured cancer cells in whole blood from healthy donors. The stretching profiles of chip designs with different length of straight channels and with/without herringbones were characterized by visualizing an aliquot, indicating purity was enhanced by stretching the aliquot severely.

The third chapter focuses on utilizing a S-eDAR platform for rare cell isolation from PBMCs. Due to the low abundance of rare cells, a large volume of blood is usually run to isolate enough numbers of rare cells for the downstream analysis, which brings a concern on the cost of time and antibodies. To save the cost of time and antibodies, PBMCs were isolated from

whole blood, concentrated in a relatively small volume, and tested by the S-eDAR platform. With the maximal concentration (100 million/mL) of PBMCs, the cost was only 1/20 of the whole blood sample which contains same amount of white blood cells. We further isolated fetal nucleated red blood cells (fNRBCs) from cord blood and tested specific markers including CD71, fetal-HbF and CD45 to characterize fNRBCs. Single-cell FISH analysis was performed with a micromanipulator by picking up single cells after they were collected in a well-plate, demonstrating the facile downstream analysis following the S-eDAR platform. FISH analysis on these fNRBCs was successfully carried out, with one red dot indicating the SRY gene on the Y chromosome. At the end, fNRBCs (CD71+, HbF+, DAPI+ and CD45-) were successfully enriched from PBMCs of the 2nd trimester maternal blood samples.

The fourth chapter introduces the home-built single molecule sensitivity flow setup for surface protein profiling on exosomes. First, the technique was validated with single molecules including alexa647-anti-IgG and PE-anti-IgG. Then it was applied to characterize protein profiling on DiFi EVs with 3 tetraspanin proteins, including CD9, CD63 and CD81, and EGFR. With multiplex protein labeling, this technique can be applied to detect EV subpopulations. Since this technique can be readily applied to profile surface proteins of exosomes from various origins, including cancer, to complement CTCs analysis and characterize the dynamic change of tumors, it will be beneficial for early detection of cancers. Furthermore, it can be applied for prenatal, neurodegenerative, cardiovascular, and immune diseases.

Chapter 2 Isolating Rare Cells and Circulating Tumor Cells with High Purity by Sequential eDAR

2.1 Abstract

Isolation and analysis of circulating tumor cells (CTCs) from the blood of patients at risk of metastatic cancers is a promising approach to improving cancer treatment. However, CTC isolation is difficult due to low CTC abundance and heterogeneity. Previously we reported an ensemble-decision aliquot ranking (eDAR) platform for the rare cell and CTC isolation with high throughput, greater than 90% recovery, and high sensitivity, allowing detection of low surface antigen-expressing cells linked to metastasis. Here we demonstrate a sequential eDAR platform capable of isolating rare cells from whole blood with high purity. This improvement in purity is achieved by using a sequential sorting and flow stretching design in which whole blood is sorted and fluid elements are stretched using herringbone features and the parabolic flow profile being sorted a second time. This platform can be used to collect single CTCs in a multi-well plate for downstream analysis.

2.2 Introduction

Most cancer deaths are due to tumor metastasis. Circulating tumor cells (CTCs) are precursors to metastasis shed from the primary tumor and present in the blood in extremely low numbers. Because of the role CTCs play in metastasis, isolating these cells from blood is an important area of research. CTCs can be isolated from blood cells based on physical and molecular differences; however, owing to their low abundance (tens to hundreds per ml of whole blood)[9-11] and heterogeneity,[12] detection and isolation is difficult.

A variety of approaches to isolate CTCs have been used, falling into two main categories: physical isolation and biomarker/antibody-based methods. Physical isolation methods are based on differences in the cell size or other physical characteristics. For example, CTCs are typically larger than blood cells and can be isolated by filtration[14, 15, 17, 66, 67] or flow fractionation.[19] Filtration is fast and simple but there is overlap in CTC and white blood cell (WBC) sizes,[20] causing low purity; in addition, the deformability of CTCs makes them difficult to be removed from the filter. Differential flow patterns of cells in microfluidic channels have been used to isolate CTCs from blood cells,[21] but this approach also often results in low purity and can be complicated to implement. Dielectrophoretic detection methods[22] based on structural differences between CTCs and WBCs (including size) require further development to achieve high purity.

Antibody-based methods have the potential to isolate CTCs with high purity due to the specificity of antibodies. As examples, the following three antibody-based approaches have

been used: (1) Immunomagnetic isolation: a blood sample is labeled with anti-CTC/epithelial-cell antibodies immobilized to magnetic beads and a magnetic field is applied to separate antibody-bound CTCs/epithelial cells.[23-25] CellSearch®, the main FDA-approved CTC detection platform, employs immunomagnetic isolation, but it is unclear whether this method has sufficient sensitivity to detect CTCs expressing low levels of surface antigen. (2) Surface capture: CTCs are captured by antibodies immobilized on the surface of a microfluidic chip.[27-30] The sensitivity of this approach was low initially due to insufficient contact of CTCs with chip features in the laminar flow, but advances using engineered microfluidic flow patterns, such as with herringbone (HB) structures to increase mixing, have greatly improved outcome.[31, 32] (3) Fluorescence-based methods: blood is labeled with fluorescent anti-CTC antibodies and CTCs are detected using laser-induced fluorescence. Fluorescence methods are promising due to their high sensitivity[33] and will continue to improve with advances in fluorescent probe brightness.

We have previously developed an ensemble decision aliquot ranking (eDAR) platform for isolating rare cells and CTCs from whole blood. The rare-cell isolation platform consists of an optical detection system, a microfluidic active sorting scheme, and an on-chip filter for cell enumeration. The optical detection system uses laser-induced fluorescence detection across the width of a microfluidic channel.[36] Labeled cells in whole blood samples can be detected in multiple colors and enumerated from detection traces.[35] The sorting scheme consists of a junction where upon detection, CTCs are diverted to a channel leading to

on-chip filters. Trapped cells can be fixed, permeabilized, and labeled with antibodies prior to enumeration. Recent improvements in this platform include a dual-capture scheme in which two subsets of rare cells can be sent to two separate filters on the microchip[37]; a sequential bleaching and relabeling scheme for highly multiplexed analysis of biomarkers on CTCs[68]; a method to calibrate and determine the limit of detection and quantitation of eDAR in terms of the number of required surface antigens; and improved detection of cells expressing low levels of the CTC marker, EpCAM.[33]

High-sensitivity recovery and purity are essential for successful CTC isolation and analysis. Collecting functionally viable cells for downstream analysis is also important for assessing CTC heterogeneity. High-sensitivity detection is important because cells expressing low levels of surface antigen have been linked to metastasis.[69] Our eDAR platform has previously demonstrated high recovery rates of viable CTCs, including those expressing low levels of cell-surface biomarkers, such as EpCAM. To keep CTCs amenable to biological characterization, like genomic or transcriptomic analyses after isolation, high purity is needed, since neighboring hematologic cells may complicate readout and analysis.

Here we describe the ability to isolate CTCs with high purity using a sequential two-stage eDAR sorting in which a blood aliquot is first sorted, then stretched, and then sorted a second time to isolate the single CTC of interest. The flow-stretching element together with the second sorting step can improve the purity by 70-fold. Because these additional steps occur on the same chip, minimal additional time is needed; 1 ml of blood can be run through a chip

in 20 minutes and single CTCs can be collected in wells of a multi-well plate for imaging and analysis.

2.3 Experimental Section

2.3.1 Cell Culture

MCF-7 human breast cancer cells were obtained from American Type Culture Collection (ATCC, Manassas, VA). Cells were cultured at 37°C and 5% CO2 in EMEM media (ATCC) supplemented with 5% fetal bovine serum and 1% penicillin/streptomycin (Sigma, St. Louis, MO).

2.3.2 Reagents and Materials

Healthy whole blood samples were obtained from PlasmaLab International (Everett, WA). DAPI Solution (1 mg/ml) was purchased from Thermo Fisher Scientific (Waltham, MA). Antibodies were purchased from BioLegend, Inc. (San Diego, CA) and included phycoerythrin (PE)-anti-human EpCAM, Alexa Fluor 647 anti-human cytokeratin (pan reactive), Alexa Fluor 488 anti-human CD45, PE anti-human CD45 and PE goat anti-mouse IgG. Isoton II buffer (Beckman Coulter, Brea, CA) was used as a sheath flow for eDAR chips. A solution of 1% bovine serum albumin (BSA; Sigma) / 0.05% Tween 20 (Sigma) in Isoton II buffer was used to pretreat multi-well plates (Cellvis, Mountain View, CA) and PTFE tubing (SAI Infusion Technologies, Lake Villa, IL). Isoton II buffer with 0.1% BSA was used for labeling cells. A solution of 25% glycerol (EMD, Billerica, MA) in Isoton II buffer was used to simulate the fluidic characteristics of blood for testing sorting and aliquot stretching, and

was mixed 30:70 with green food dye (COV Extract Company, Rockford, OH) for bright-field imaging. Yellow fluorescent beads were purchased from Duke Scientific (Palo Alto, CA).

2.3.3 Microfluidic Chips

Silicon masters were created using standard photolithographic techniques. SU-8 2050 photoresist (MicroChem, Westborough, MA) was used for spin coating. Chips were made using PDMS with a 1:10 ratio of precursor to polymer base. PDMS was cured and sealed to a glass substrate immediately following exposure to O_2 plasma for 30 seconds. If not used immediately, chips were covered and stored for up to one month until use.

2.3.4 Cell Recovery Measurements

MCF-7 cells ($1x10^6$/ml) were labeled with PE-anti-EpCAM (0.5 µg/ml) for 1 h. After washing, cells were counted using a hemocytometer and serial diluted, and ~100 cells were spiked into 0.5 ml of blood. The sample was loaded onto a sequential sorting chip at 30 µL/min and sorting was established by adjusting the sheath flow pressure. Fresh tubing treated with 1% BSA / 0.05% Tween 20 was attached to the collection outlet and run into a pretreated well of the 96-well plate. The tubing was moved into a new well once the volume of collected solution in the previous well reached ~250 µl. The total output for sorting 0.5 ml of blood was ~1 ml. To enumerate collected cells, the plate was spun down at 450 rcf for 10 min and PE anti-EpCAM positive cells were counted using an inverted fluorescent microscope with a 20X 0.75 NA objective (Nikon, Tokyo, Japan). MCF-7 cells stained with

PE-anti-EpCAM can be clearly identified since all other blood cells were not fluorescent. The cell recovery rate was calculated as the number of MCF-7 cells counted divided by the number of MCF-7 cells spiked into the sample.

2.3.5 Cell Identification and Purity Measurements

MCF-7 cells were labeled with PE-anti-EpCAM, spiked into a blood sample, and run on a chip as described above for cell recovery measurements. Sorted PE-labeled MCF-7 cells and unlabeled WBCs and red blood cells (RBCs) were collected in a pretreated Eppendorf tube instead of a 96-well plate. The tube was centrifuged at 450 rcf for 10 min and the supernatant aspirated. RBCs were removed by adding RBC lysis buffer and incubating for 15 min, leaving MCF-7 and WBCs intact, and the tube was centrifuged again to pellet the cells. The cells were fixed using 2% paraformaldehyde for 15 min. After centrifuging and washing twice, cells were permeabilized using 0.2% saponin and stained with Alexa Fluor 488 anti-CD45 (10 μg/ml; for identification of WBCs) and Alexa Fluor 647 anti-panCK (5 μg/ml; for identification of MCF-7 cells). DAPI (1 μg/ml) was added to stain nuclei. The cells were washed and resuspended in Isoton II buffer and transferred to a glass-bottom multi-well plate for imaging. A fluorescence microscope with a 20X objective was used for confirmation of cell identities and imaging. For the chip with the 3cm straight channel, the purity was calculated after confirming cells' identities. The labeled cells in a 384-well plate well were imaged with a 4X objective for both DAPI and PE channels and 6 images were captured and stitched together to represent the whole well. Cell purity was calculated as the number of

PE-labeled MCF-7 cells divided by the total number of DAPI-stained cells.

In addition to the use of imaging to determine cell purity as described above, we also used our eDAR chip as a flow cytometer to quantify cell purity. Here, the recovered cells were flown through the eDAR chip, and the number of MCF-7 cells and WBCs were counted. Specifically, MCF-7 cells were first labeled using PE tagged anti-EpCAM, spiked into a blood sample, and the sample was run on a chip as described above. The number of sorted MCF-7 cells was counted based on fluorescent signals triggering sorting events at the second detection line. The outlet solution was connected to a pretreated 15-ml tube, centrifuged, supernatant aspirated leaving ~300 µl, and pelleted cells were resuspended. PE tagged anti-CD45 was added to label WBCs for 1 h, so that both MCF-7 cells and WBCs were labeled with PE. After washing, the sample was run through a new eDAR chip punched only at the inlet and at one outlet, with solenoids turned off so that no sorting occurred. APD traces were collected to count the number of cells at the second detection line; the number of peaks indicated the total number of cells in the outlet solution. MCF-7 cell purity was calculated as the number of MCF-7 cells counted in the first step, divided by the total number of cells collected as counted in the second step.

2.3.6 Visualizing Aliquot Stretching Profiles

To simulate the fluid characteristics of blood, a mixture of 25% glycerol solution and Isoton II buffer was used. To test the ability of different chip designs to stretch an aliquot, filtered PE goat-anti-mouse IgG was added to the mixture to visualize aliquots sorted at the sorting

junctions in APD traces. Yellow fluorescent beads (~1500 10-μm beads) were added to the sample to trigger sorting using solenoids, and the sample was loaded onto the chip. Buffer pressures were adjusted until stable sorting at the two junctions was established. APD traces were collected, and the time required for a sorted aliquot to travel from completely through the first sorting junction to completely through the second sorting junction was measured.

2.4 Results and Discussion

2.4.1 Improving Purity by Two-stage Sequential Sorting

We designed a sequential eDAR chip with a second sorting junction to improve CTC purity with respect to WBCs (Figure 2.1). The flow at each of the two sorting junctions (Figure 2.2) was similar to that previously reported for the 1-stage eDAR sorting.[24, 25] Laser illumination lines were positioned just before each sorting junction (Figure 2.1 a, dark blue lines). After the first junction, the aliquot is stretched as it passes down a channel between two sorting junctions, and the second sorting event is triggered when labeled cells reach the second laser detection line.

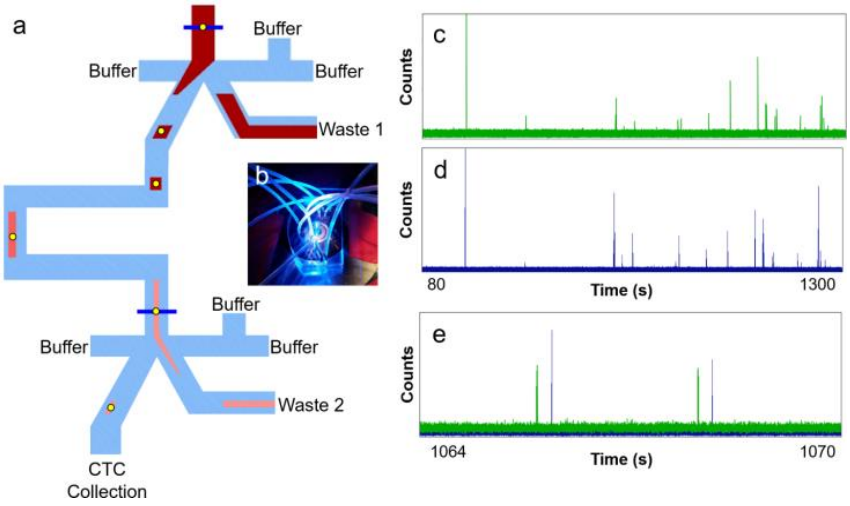

Figure 2.1 Schematic of sequential eDAR chip. (a) Blood is loaded at the inlet (top) and CTCs can be detected at two detection lines (blue) using laser-induced fluorescence. CTC-detection signals trigger sorting events at two junctions by activating solenoids and increasing the pressure of flow from the right side of the junction, causing the aliquot to flow to the left. After a target is detected at the first junction, the aliquot containing it flows to the left and passes down a channel to the second detection line, after which it is sorted a second time. The aliquot is stretched in the channel between two junctions, resulting in fewer contaminating blood cells. Unsorted blood cells are sent to waste (Waste 1 and 2). (b) Image of a sequential eDAR chip while running a sample, mounted on a microscope using a 488 nm laser excitation. c-d APD traces from the first (c) and second (d) sorting junctions in a single run. e Overlay of enlarged section from c and d, showing sorting events at the first junction (green) followed by sorting events at the second junction (blue).

APD traces from the two laser detection lines are shown in Figure 2.1 c and d, and an overlay of an enlarged section of the two traces is displayed in Figure 2.1 e, showing sequential cell

sorting events at the two junctions. During the delay between the signals from the two detection lines, the aliquot containing labelled cells is stretched and diluted. This step reduces the concentration of blood cells and improves the purity of target cells in the second sorted aliquot.

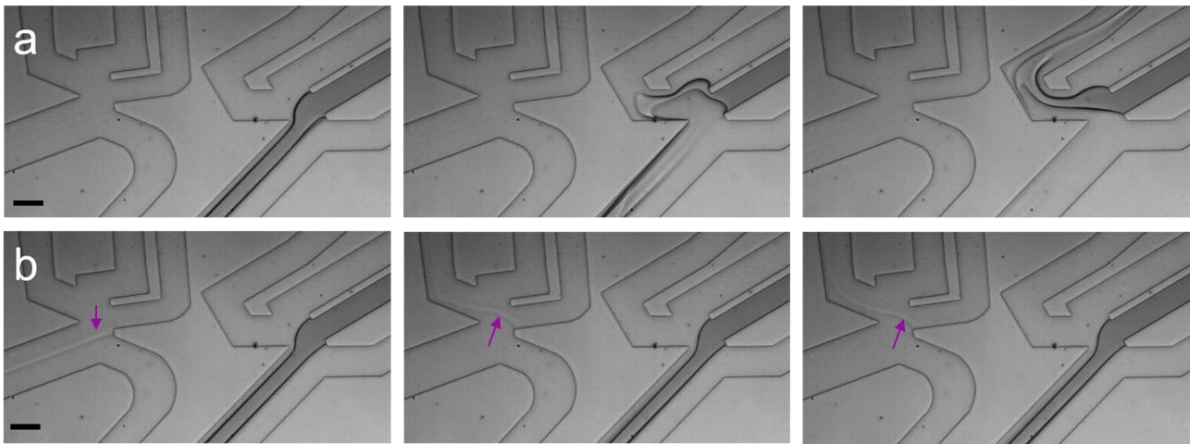

Figure 2.2 Sequential sorting fluidics scheme. The visualized flow was a mixture of 30% glycerol solution (25% glycerol in Isoton II buffer) and 70% green food dye. ***a*** *One sorting event at the first junction (right side of images). From left to right: no solenoid open; first solenoid was triggered, flow shifts left; flow fully switched to the channel connecting the two sorting junctions.* ***b*** *One sorting event at the second junction (left side of images), while the first solenoid was switched off. From left to right: no solenoid open; second solenoid was triggered, flow shifts left; flow fully switched to the collection channel. The aliquot at the second sorting junction was more difficult to visualize, indicating the aliquot was diluted further after passing through the first sorting junction. The purple arrows were used to mark flow at the second sorting junction. Scale bars are 200 µm.*

The cell recovery rate of the platform was measured previously using various cancer cell lines and clinical samples.[33, 37, 38] In the modified platform, two new elements were added, where cell loss might occur: the second sorting junction and collecting sorted cells with a 96-well plate. Recovery measurements using PE anti-human EpCAM labeled MCF-7 cells spiked into whole blood were performed to verify that these elements do not cause cell loss. Pre-labeled MCF-7 cells with bright PE fluorescence can be differentiated from unlabeled blood cells (Figure 2.4) under a fluorescent microscope and the number of MCF-7 cells recovered can be counted. For a 2-stage (2-junction) sequential sorting, the recovery rate was > 90%, as high as 1-stage sorting.[36] No observable cell loss was caused by adding a second sorting junction or by collecting sorted cells with multi-well plates. MCF-7 cell clusters can also be detected and isolated by eDAR in some cases (Figure 2.3), illustrating the capability of the system to enrich cell clusters, potentially useful for studying CTC clusters.[70]

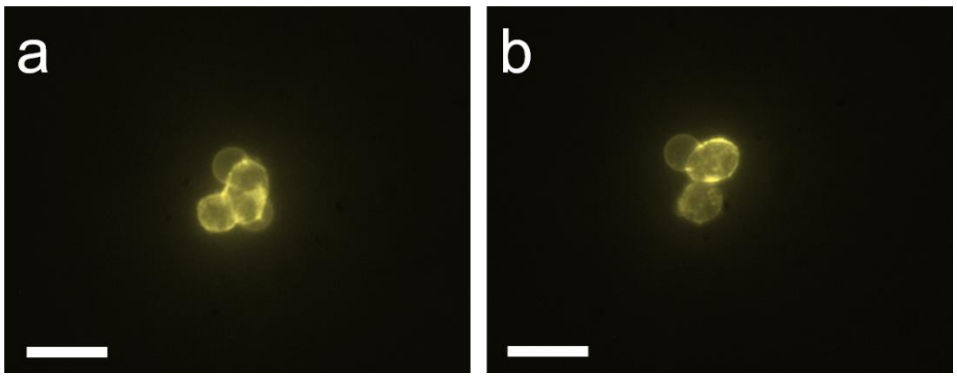

Figure 2.3 Two clusters of MCF-7 cells. MCF-7 cells were labeled with PE-anti-EpCAM and sorted into a multi-well plate using a sequential eDAR chip. Scale bars are 40 µm.

2.4.2 Cell Confirmation with Fluorescence Microscopy

To confirm the identities of sorted cells and to quantify target cell purity when using a chip with a 3 cm-long channel (with no herringbone mixing features) and two sorting junctions, sorted cells were collected in Eppendorf tubes. After that, RBCs were lysed using RBC lysis buffer and non-RBCs were fixed, permeabilized, and stained with markers including DAPI, Alexa Fluor 488 anti-human CD45, and Alexa Fluor 647 anti-human Cytokeratin (panCK). MCF-7 cells were DAPI+, CD45-, EpCAM+ and panCK+; WBCs were DAPI+, CD45+, EpCAM- and panCK- (Figure 2.4 b and c).

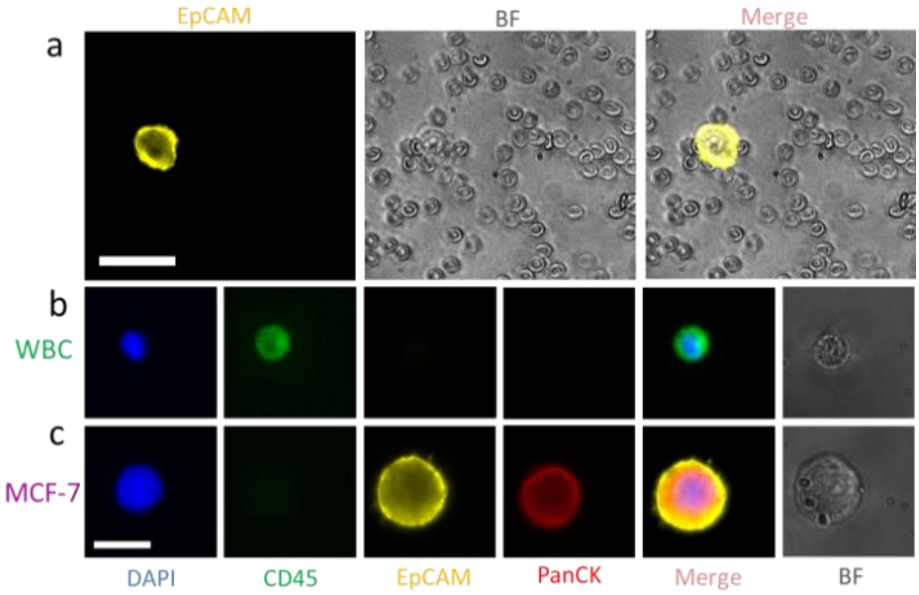

Figure 2.4 Fluorescent imaging for cell confirmation. (a) Images of collected MCF-7 cells and blood cells after sorting using sequential eDAR. Cells were imaged using a 20X 0.75 NA objective. Scale bar is 40 µm. (b-c) Confirmation of a MCF-7 cell and a WBC identity. MCF-7 cells are DAPI+, CD45-, EpCAM+, panCK+; WBCs are DAPI+, CD45+, EpCAM-, panCK-. Scale bar is 20 µm.

Purity was calculated by counting the number of PE-labeled MCF-7 cells and dividing by the total number of DAPI-labeled cells. To image an entire well of the 384-well plate, six images captured with a 4X objective under both DAPI and PE channels were stitched together (Figure 2.5). With this chip and the particular operating protocol, the CTC purity achieved using a 3-cm channel, 2-stage chip was ~15%.

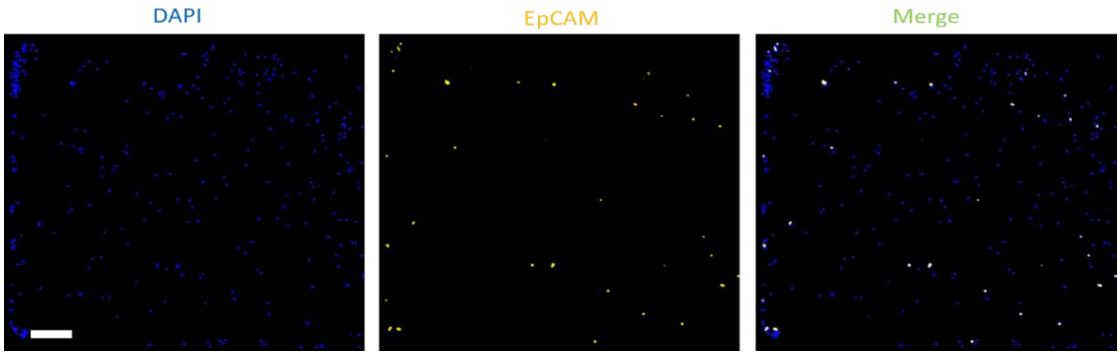

Figure 2.5 Fluorescent images of collected cells after sorting with a 2-stage 3 cm-channel chip. DAPI (blue) channel showed cell nuclei of collected cells and PE-EpCAM (yellow) channel showed MCF-7 cells. The scale bar is 500 μm.

2.4.3 Purity Test with the S-eDAR Platform

Using the alternate method to measure cell purity, based on the number of cell sorting events detected (see Methods), the MCF-7 cell purity using a 3 cm-channel, 2-stage sorting chip was 17%, similar to the 15% purity calculated by counting cells using fluorescence microscopy. In Figure 2.6, panels on the left show the complete trace records for MCF-7 cells (labeled with PE tagged anti-EpCAM). Panels on the right show the complete trace records for MCF-7 cells plus WBCs (labeled with PE tagged anti-EpCAM and anti-CD45). Using the

same method, the previous chip with only one sorting junction achieved only ~1% cell purity for this particular chip and current operating condition, shown in Figure 2.7 (e.g., we did not use the fastest possible sorting speed in the first junction). Thus, a large (17-fold) improvement in MCF-7 cell purity was achieved for 2-stage versus 1-stage eDAR sorting.

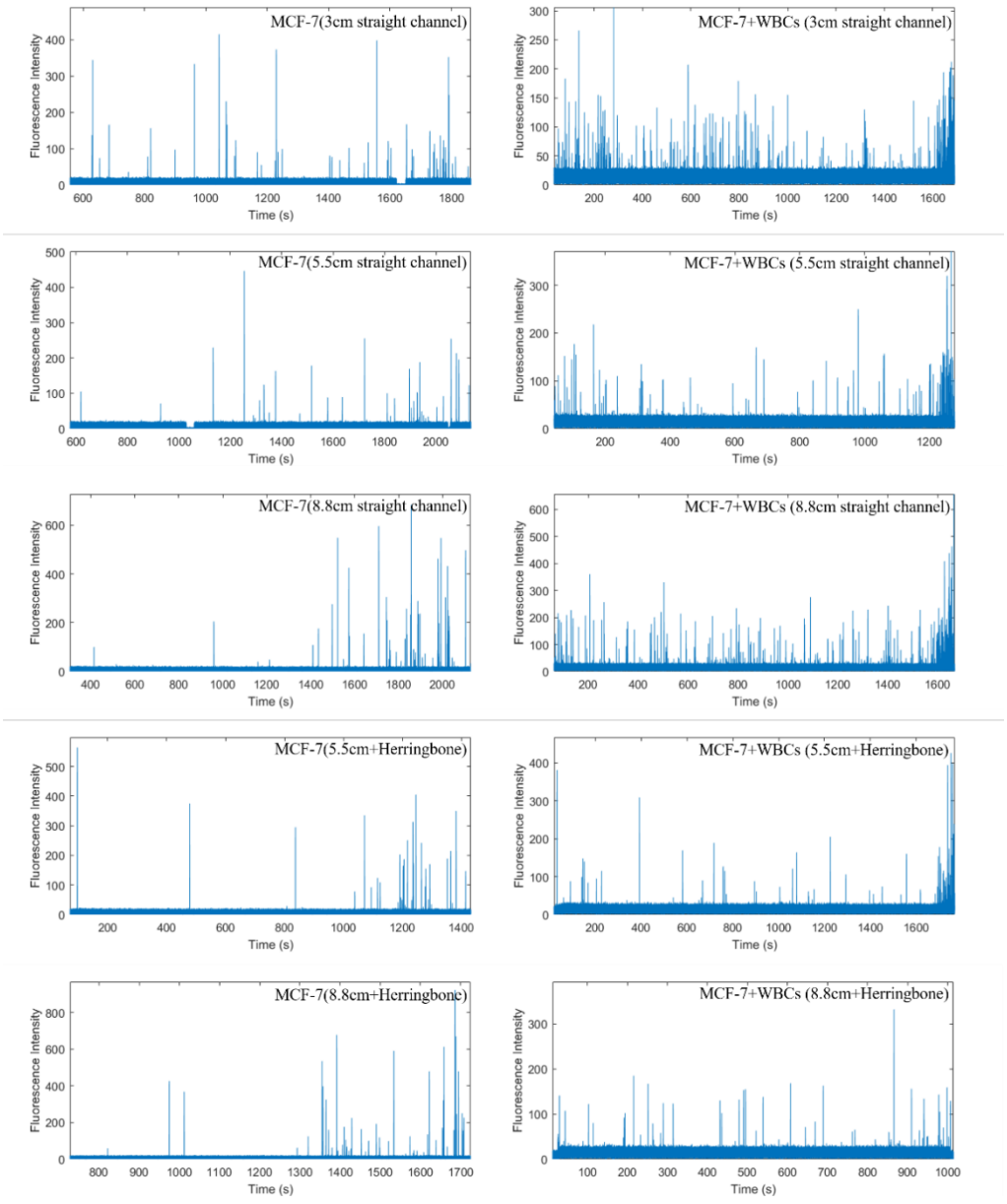

Figure 2.6 Counting and quantifying the number of MCF-7 cells and total nucleated white blood cells with S-eDAR. (MCF-7+WBCs) collected from five chips with different

flow-stretching channels: 3cm straight channel, 5.5cm straight channel, 8.8cm straight channel, 5.5cm+Herringbone and 8.8cm+Herringbone. Panels on the left show the complete trace records for MCF-7 cells (labeled with PE tagged anti-EpCAM). Panels on the right show the complete trace records for MCF-7 cells plus WBCs (labeled with PE tagged anti-EpCAM and anti-CD45).

2.4.4 Lengthening the Sorting Channel to Improve Cell Purity

Dispersion of the cell aliquot by diffusion in microchannel is extremely low. The main mechanism that stretches out the cells in flow is axial dispersion caused by the parabolic flow profile. As a result, a longer channel should enhance separation of the cells within the aliquot, thereby improving the target cell purity. To test this hypothesis, two chips with longer channels (5.5 cm and 8.8 cm) between the two sorting junctions were designed, and MCF-7 cell purity was measured with S-eDAR as described above. The 5.5 cm and 8.8 cm channels yielded purities of 21% and 32%, respectively (Table 2.1).

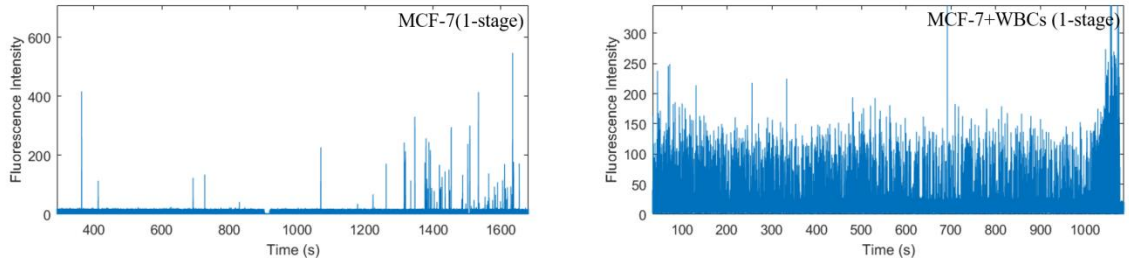

Figure 2.7 Counting and quantifying the number of MCF-7 cells and total nucleated white blood cells (MCF-7+WBCs) with only one sorting stage. The panel on the left shows the complete trace records for MCF-7 cells (labeled with PE tagged anti-EpCAM). The panel on

the right shows the complete trace records for MCF-7 cells plus WBCs (labeled with PE tagged anti-EpCAM and anti-CD45). The purity of MCF-7 cells is around 1%.

Table 2.1 Tabulation of the number of spiked-in MCF-7 cells and WBCs that were recovered from five sequential eDAR chips of different flow-stretching designs.

	3cm	5.5cm	8.8cm	5.5cm+HB	8.8cm+HB
MCF-7	54	29	57	30	49
MCF-7+WBCs	313	141	177	100	70
Purity	17.3%	20.6%	32.2%	30.0%	70.0%

2.4.5 Mixing Features Further Improves Cell Purity

Lengthening the sorting channel between junctions from 3 cm to 8.8 cm yielded a modest improvement in purity, from 17% to 32%. To achieve further improvement, we tested two additional approaches to stretch an aliquot: (1) “flow sharers”, in which the main channel is connected to a series of smaller channels such that part of the aliquot would travel down the first small channel and part would continue down the main channel, to separate the aliquot into many smaller fluid elements, and (2) herringbone features (Figure 2.8 a and b). Aliquot stretching profiles of three channel designs were assessed by measuring the duration of the PE signal at the second detection line (Figure 2.8 c). Greater aliquot stretching was expected to result in fewer contaminating blood cells accompanying MCF-7 cells during sorting events. The first flow stretching design, using small side channels, resulted in an increase in stretching, but when tested with whole blood, clogging occurred, indicating potential cell loss.

Clogging was prone to occur due to the presence of the narrow channels that were meant to spread out the plug of cells because an occasional cluster of cells could block the narrow channels and then the device would function less efficiently. The second flow stretching design, using herring-bone features, resulted in greater stretching and no clogging. Thus, in subsequent experiments we tested different lengths of straight channels with herringbones structures in cell purity measurements.

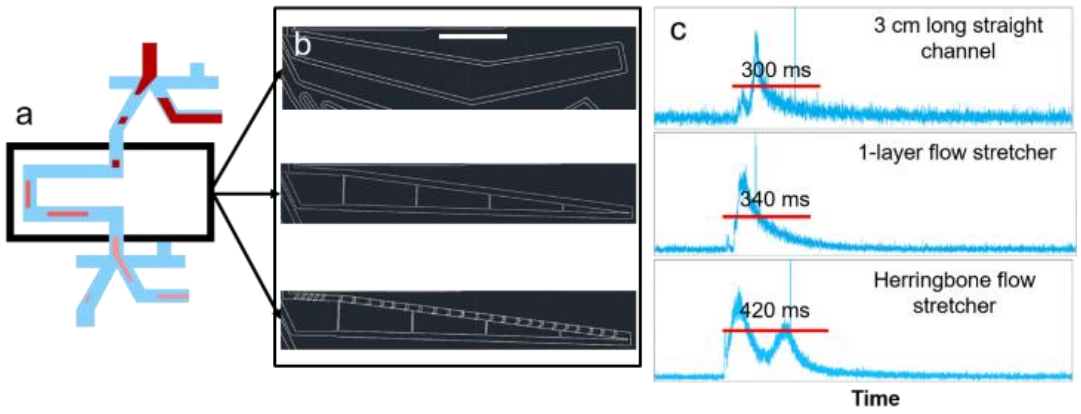

Figure 2.8 Aliquot stretching using different channel designs. ***a*** *Three chip designs were the same except for the channel separating two sorting junctions.* ***b*** *Three designs of the channel separating two sorting junctions by AutoCAD. From top to bottom: basic straight channel, adding "flow sharers", adding "flow sharers" and herringbone structures. Except for the small narrow channels in the "flow sharer" designs, the width of the straight channels was around 200 µm and the height was kept the same for each design (i.e. 50 µm). The scale bar is 3 mm. c APD traces of aliquots containing PE dye and yellow fluorescent beads triggering sorting events at the first sorting junction, were recorded at the second detection line. The duration of the PE signal of one aliquot at the second detection line was used as an indicator of*

the degree of aliquot stretching.

Herringbones were first described by Whitesides and coworkers in 2002[32] are attractive as a mixing strategy, they are simple to fabricate, tunable to a wide variety of applications,[71] and do not trap cells. Here, lateral mixing enhanced axial dispersion of the cells because it caused the cells to sample actively different portions of the parabolic flow profile. We used herringbone features located at the beginning (first 0.7 cm) of the 5.5 cm and 8.8 cm channels connecting the junctions to mix, which spread the aliquot laterally before it reached the second junction.

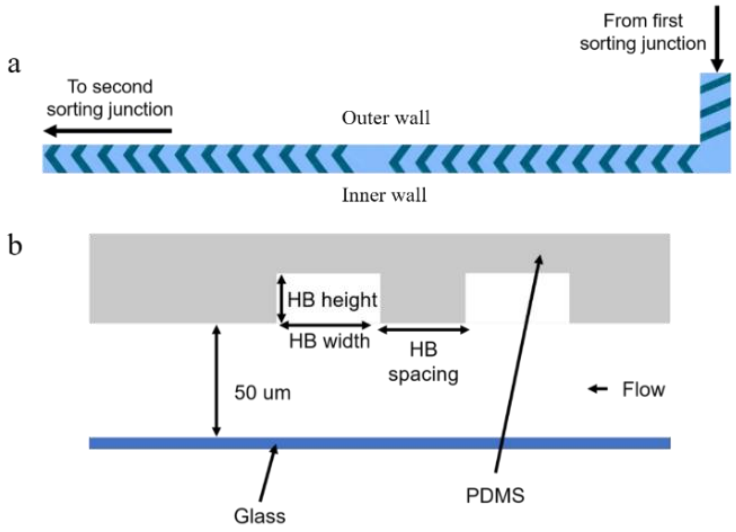

Figure 2.9 ***a*** *Schematic of herringbone structures.* ***b*** *Cross-section of the channel with herringbones. For staggered herringbones, the height was 30 µm and the width was 70 µm. For straight ridges at the beginning of this channel, the height was 30 µm and the width was 80 µm; spacing was 180 µm for staggered herringbones and 95 µm for straight ridges.*

The herringbone design consisted of three sections (Figure 2.9 a): (1) 3 straight ridges angled

from the inner wall to the outer wall, since we had observed the aliquot traveling primarily down the inner wall; (2) 12 staggered HB angled slightly toward the inner wall, and (3) 12 staggered HB angled slightly toward the outer wall. The herringbone dimensions are described in Figure 2.9 b. The mixing section was 0.7 cm long, followed by a 4.8 cm or 8.1 cm straight channel. Without herringbones, the aliquot traveled as a plug along the outer wall; with herringbones, the aliquot was spread laterally across the channel. The long section of the straight channel without herringbones would be expected to allow further longitudinal separation of cells by axial dispersion due to the parabolic flow profile, as cells near the center of the channel travel faster than those near the outer edges.

The 5.5 cm herringbone chip yielded 30% cell purity. Furthermore, the 8.8 cm chip with herringbones yielded 70% purity, which corresponds to an average of <1 WBC per CTC sorted (Figure 2.4). Cell purity results for different chip designs are summarized in Table 2.1. APD traces for counting and quantifying the number of MCF-7 cells and total nucleated white blood cells (MCF-7+WBCs) were collected from five chips with different flow-stretching channels, shown in Figure 2.6.

The herringbone design consisted of three sections (Figure 4a): (1) 3 straight ridges angled from the inner wall to the outer wall, since we had observed the aliquot traveling primarily down the inner wall; (2) 12 staggered HB angled slightly toward the inner wall, and (3) 12 staggered HB angled slightly toward the outer wall. The herringbone dimensions are described in Figure 4b. The mixing section was 0.7 cm long, followed by a 4.8 cm or 8.1 cm

straight channel. Without herringbones, the aliquot traveled as a plug along the outer wall; with herringbones, the aliquot was spread laterally across the channel. The long section of the straight channel without herringbones would be expected to allow further longitudinal separation of cells by axial dispersion due to the parabolic flow profile, as cells near the center of the channel travel faster than those near the outer edges.

2.4.6 Characterizing Aliquot Stretching Profiles

The aliquot stretching profiles of four designs with various lengths of channels and mixing features (3 cm, 5.5 cm, 5.5 cm + HB, and 8.8 cm + HB) are shown in Figure 2.10. Longer channels and addition of herringbone features resulted in longer durations of PE signals, indicating greater aliquot stretching. For the 8.8cm +HB chip, the duration of an aliquot passing through the second detection line increased to 1500 ms, with decreased intensity of PE signals, which indicates the aliquot was diluted and stretched with addition of a 8cm channel and herringbone structures.

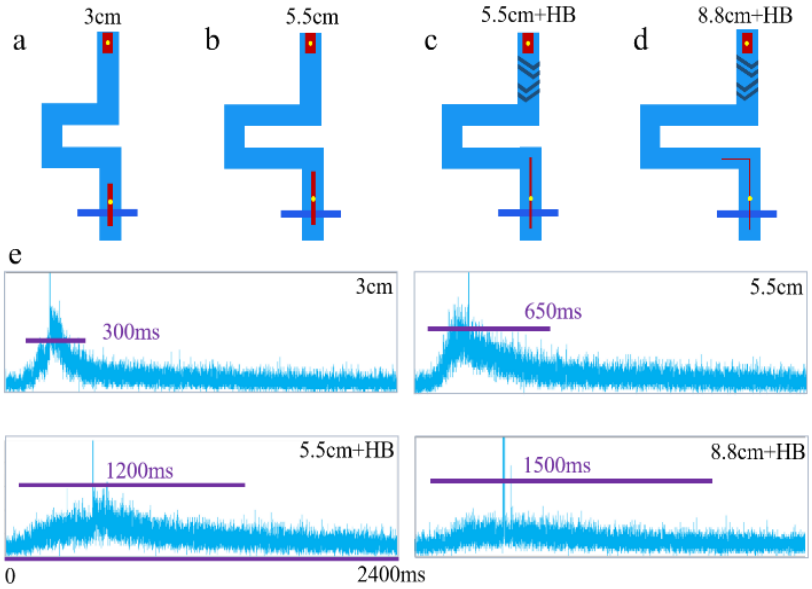

Figure 2.10 Aliquot stretching using different chip designs. (a) 3 cm channel, (b) 5.5 cm channel, (c) 5.5 cm channel with HB, (d) 8.8 cm channel with HB. (e) APD traces for the aliquots containing PE dye and fluorescent beads at second detection line. The spikes in four images indicated that fluorescent beads triggered sorting at the first sorting junction and passed through the second detection line, along with the aliquot.

2.5 Conclusions

In this study we described a platform for isolating CTCs with high purity with respect to WBCs by using sequential sorting and fluidic features for aliquot stretching. We achieved a roughly 70-fold improvement in target cell purity compared to our previous eDAR platform, by using two sorting junctions, a longer channel between junctions, and herringbone features to enhance lateral mixing and spreading of the cells. We also moved cell collection off-chip while maintaining a high cell recovery rate. Single CTCs now can be collected in wells of a

multi-well plate with less than one contaminating WBC, on average, making eDAR amenable to downstream analyses such as PCR or DNA sequencing. Future development of this platform will couple it with automated dispensing to allow single CTC detection, enumeration, and analysis with high sensitivity, cell recovery, and purity, and for isolating and characterizing low surface antigen-expressing metastatic cells that may be missed by other methods. Further optimization of the fluidic stretcher should result in additional purity improvements.

Chapter 3 Sequential eDAR Isolation and FISH Identification of Rare Cells from Blood by Using Concentrated Peripheral Blood Mononuclear Cells

3.1 Abstract

Isolation and analysis of circulating rare cells is a promising approach for early detection of cancer and other diseases and for prenatal diagnosis. Isolation of rare cells is usually difficult due to their heterogeneity as well as their low abundance in peripheral blood. We previously reported a two-stage ensemble-decision aliquot ranking platform (S-eDAR) for isolating circulating tumor cells from whole blood with high throughput, high recovery rate (>90%), and good purity (>70%), allowing detection of low surface antigen-expressing cancer cells linked to metastasis. However, due to the scarcity of these cells, large sample volumes and large quantities of antibodies were required to isolate sufficient cells for downstream analysis. Here we drastically increased the number of nucleated cells analyzed by first concentrating

peripheral blood mononuclear cells (PBMCs) from whole blood by density gradient centrifugation. The S-eDAR platform was capable of isolating rare cells from concentrated PBMCs (10^8/mL-equivalent to processing ~20 mL of whole blood in the 1 mL sample volume used by our instrument) at a high recovery rate (>85%). We then applied the S-eDAR platform to isolating rare fetal nucleated red blood cells (fNRBCs) from concentrated PBMCs spiked with umbilical cord blood cells and confirmed fNRBC recovery by immunostaining and fluorescence in situ hybridization, demonstrating the potential of the S-eDAR system for isolating rare fetal cells from maternal PBMCs to improve noninvasive prenatal diagnosis.

3.2 Introduction

Circulating rare cells are attractive for use in prognosis of cancer and viral infections and in prenatal diagnosis.[72] However, detection and isolation of circulating rare cells is difficult due to their scarcity[9-11, 73] and heterogeneity in expression of surface markers.[12, 21] Approaches to isolating rare cells fall into two categories: label-free methods and affinity or antibody-based methods.[74] Label-free isolation methods exploit differences in cell size,[75-77] density,[78] deformability,[79] and dielectric properties.[22, 80, 81] Because some rare cells such as some circulating tumor cells (CTCs) are larger than white blood cells (WBCs), they can be isolated by filtration.[15, 22] However, the overlap in the sizes of rare cells and WBCs[20] can yield low cell purity following filtration. Label-free approaches to cell isolation also suffer from low recovery, clogging of filters, complicated integration of external force fields, and loss of cell

viability, limiting their utility.[82]

Antibody-based methods can be employed to isolate rare cells based on expression of surface marker proteins. Three common antibody-based approaches are: (1) immune-magnetic isolation, in which rare cells are captured by antibodies immobilized to magnetic beads that are separated by a magnetic field;[23, 25] (2) microfluidics approaches[25] in which rare cells are captured by antibodies immobilized on a microfluidic chip;[28, 29] and (3) fluorescence -activated methods in which rare cells are incubated with fluorophore-labeled antibodies and the cells are detected and sorted based on sensitive laser-induced fluorescence.[33, 83]

Fetal cells in maternal blood during pregnancy are potentially useful for noninvasive prenatal diagnosis because they contain the whole fetal genome, uncontaminated with maternal DNA.[38] Fetal cell types present in maternal blood during pregnancy include myeloid fetal progenitor cells, fetal lymphocytes, syncytiotrophoblasts, fNRBCs, and circulating extravillous trophoblasts (CTBs).[39-41] Fetal lymphocytes and myeloid fetal progenitor cells are poor candidates for prenatal diagnosis because they persist in maternal blood for years after pregnancies, causing contamination from previous pregnancies.[43] Syncytiotrophoblasts-large, multinucleated placental epithelial cells shed into the maternal circulation during the first trimester, are poor targets for prenatal diagnosis, because they become trapped in lung capillaries and are removed from circulation.[44] CTBs are a promising target for early fetal diagnosis because their short lifespan precludes contamination from previous pregnancies; however, they are extremely rare and methods to enrich them lacked

consistency and repeatability. Furthermore, confined placental mosaicism is an obstacle to interpret the results obtained by analyzing CTBs. The fNRBCs are a promising cell type for noninvasive prenatal testing with short life span (25-35 day half-life in adult circulation) preventing contamination from previous pregnancies. fNRBCs are abundant in fetal blood early in gestation,[47, 48] but they are rare in maternal peripheral blood with a reported occurrence ranging from 3-26 cells per mL.[49-51] They have been successfully enriched from maternal blood by MACS,[52] FACS,[53] and microfluidics techniques.[54]

In 1990, Bianchi etc. reported fNRBCs were successfully isolated from the mononuclear cell layer by FACS with anti-CD71 and the presence of fetal hemoglobin and Y chromosome sequences proved that sorted cells were fetal in origin.[53] Since then, various enrichment and confirmation methods for fetal nucleated red blood cells were developed. A combination of various antibodies, like anti-CD36, anti-CD71 and anti-GPA was applied to sort fNRBCs by FACS, since only CD71 might not be enough to isolate fNRBCs.[84, 85] Another method, immunocapture, similar as MACS, which applied microbead-based selective sedimentation to realize highly sensitive and rapid isolation of fNRBCs.[60]

He, etc. functionalized the surface of microchip with anti-CD147 to capture fNRBCs from peripheral maternal blood.[54] 3D nanostructures had the benefits to increase antibody bioconjugation and enhance the local topological cell-microchip interactions. The number of fNRBCs was quantified as the gestational age increased, showing a potential to monitor the healthy status of fetuses during the whole pregnancy. Nanosturcture microchips were utilized

to capturing fNRBCs for non-invasive prenatal diagnosis of chromosomal aneuploides and microdeletion syndrome.[56] Even though fNRBCs has been well established by developing enrichment and confirmation methods, but some disadvantages still exist. For example, high contamination with MACS, low recovery rate with FACS and time-consuming on fabricating microfluidic chips or releasing step. A facile way to isolate and collect interested cells for downstream analysis is demanding.

We previously developed an ensemble-decision aliquot ranking (eDAR) platform to isolate CTCs from whole blood which showed higher sensitivity than the FDA-approved Cell-Search platform.[36] The eDAR platform includes an optical detection system, a microfluidic active cell sorting scheme, and an on-chip filter for cell enumeration. Fluorescently labeled cells in whole blood samples can be tracked in multiple color channels and enumerated from avalanche photodiode (APD) detection traces.[35] Upon detection, CTCs are diverted to a channel that leads to an on-chip filter, where they can be fixed, permeabilized, and labeled with confirmation antibodies prior to enumeration, or diverted to a collection well or tube for downstream analysis. A high CTC recovery rate (>90%) was achieved with the eDAR platform. The eDAR platform was further improved to allow sequential sorting (S-eDAR) by using a two-stage sorting technique, which increased the CTC purity from 1% to 70%.[83]

Here we increased the number of nucleated cells analyzed with S-eDAR by first concentrating PBMCs from whole blood by density gradient centrifugation. We then used

S-eDAR to isolate rare cells from concentrated PBMCs to characterize its performance in terms of rare cell recovery rate and signal-to-noise ratio (SNR). We also developed a process to analyze cells isolated by S-eDAR with fluorescence in situ hybridization (FISH). We then applied the S-eDAR platform to isolating fNRBCs from concentrated adult female PBMCs spiked with umbilical cord blood cells to demonstrate the potential of S-eDAR for isolating rare fetal cells from maternal blood for noninvasive prenatal diagnosis.

3.3 Experimental Section

3.3.1 Cell Culture

MCF-7 cells (ATCC, Manassas, VA) were used as rare cell surrogates and were spiked into concentrated PBMC samples. MCF-7 cells were cultured at 37 °C and 5% CO_2 in EMEM media (ATCC) supplemented with 5% fetal bovine serum and 1% penicillin/streptomycin (Sigma-Aldrich, St. Louis, MO).

3.3.2 Reagents and Materials

Whole blood samples from healthy donors were obtained from PlasmaLab International (Everett, WA). Umbilical cord blood samples from women delivering male fetuses were obtained from UW Medicine following regulations of the University of Washington Institutional Review Board. All patients provided informed consent and the research was approved by the University of Washing-ton Ethics Committee. All blood specimens were collected in anti-coagulant tubes and processed within 6 h.

DAPI (1 mg/mL) was purchased from Thermo Fisher Scientific (Waltham, MA). Antibodies

used included phycoerythrin (PE)-anti-human EpCAM (BioLegend, Inc., San Diego, CA), Alexa Fluor 488 anti-human CD45 (BioLegend), PE-anti-human CD71 (Thermo Fisher Scientific, Waltham, MA), and APC-fetal hemoglobin monoclonal antibody (HbF; Thermo Fisher Scientific). Isoton II buffer (Beckman Coulter, Brea, CA) was used as sheath flow for eDAR chips. A solution of 1% bovine serum albumin (BSA; Sigma-Aldrich) / 0.05% Tween 20 (Sigma-Aldrich) in Isoton II buffer was used to pretreat glass-bottom multi-well plates (Cellvis, Mountain View, CA) and polytetrafluoroethylene tubing (SAI Infusion Technologies, Lake Villa, IL). Isoton II buffer with 0.1% BSA was used for labeling cells. Ficoll-Paque PLUS (Sigma-Aldrich) was used as the density gradient centrifugation medium for isolation of PBMCs. SRY FISH probes were purchased from Cytocell (Tarrytown, NY).

Microfluidic chips. Silicon masters were created by using standard photolithographic techniques described previously.[86] SU-8 2050 photoresist (MicroChem, Westborough, MA) was used for spin coating. To fabricate microfluidic chips, polydi-methylsiloxane (PDMS) with a 1:10 ratio of precursor to polymer base was cured and sealed to a glass substrate immediately after exposure to O_2 plasma for 30 s. If not used immediately, chips were covered and stored for up to one month until use.

3.3.3 Isolating PBMCs by Density Gradient Centrifugation

A 2-mL sample of whole blood was diluted with an equal volume of phosphate-buffered saline (PBS) and was carefully layered onto 3 mL of Ficoll-Paque PLUS. The sample was centrifuged at 400 g for 30 min at RT and the upper layer was removed, leaving the

lymphocyte layer undisturbed at the interface. The lymphocyte layer was transferred to a clean centrifuge tube and was washed twice with PBS. Mononuclear cells from cord blood were isolated by the same procedure.

3.3.4 Cell Recovery Measurements

MCF-7 cells (1×10^6/mL) were labeled with PE-anti-EpCAM antibody at 0.5 μg/mL for 0.5 h. Cells were washed, counted with a hemocytometer, and serial diluted. 50-500 cells were spiked into whole blood or into PBMCs at PBMC densities ranging from 2×10^6/mL to 1×10^8/mL. To establish stable sorting at two junctions before running cell samples, Isoton II buffer mixed with green food dye (COV Extract Company, Rockford, OH) was run on a sequential sorting chip at 30 μL/min, and stable sorting pro-files were established by adjusting the sheath flow pressure with bright-field microscopy. After stable sorting events were observed, APD traces were recorded for the remaining samples containing PBMCs. When collecting sorted cells in a multi-well plate, fresh tubing treated with 1% BSA / 0.05% Tween 20 was attached to the collection outlet and run into a pretreat-ed well. To enumerate collected cells, the plate was spun at 450 g for 10 min and PE-anti-EpCAM-positive cells were counted with an inverted fluorescence microscope and a 20× 0.75 NA objective (Nikon, Tokyo, Japan). The cell recovery rate was calculated as the number of counted MCF-7 cells divided by the number of MCF-7 cells spiked into the sample.

3.3.5 On-chip and Single-cell FISH

Female PBMCs were analyzed by S-eDAR with filters for on-chip FISH. Once female

PBMCs were loaded into an eDAR chip, sorting events were triggered by switching two solenoids controlling sorting events at two sorting junctions, and sorted cells remained in the filters. Captured cells were fixed with 3:1 methanol:acetic acid solution for 10 min and were washed twice with 2× saline sodium citrate (SSC) buffer. The cells were then dehydrated in a series of 70%, 85%, and 100% ethanol solutions in water. A 10 μL volume of probe mixture was infused into the filters containing fixed, sorted cells. The sample and probe were denatured simultaneously by heating the chip on a hotplate at 75 ºC for 2 min. The chip was then placed in a humid, opaque container at 37 ºC overnight. The cells were washed with 0.4× SSC at 72 ºC for 2 min, then with 2× SSC buffer, 0.05% Tween-20 at room temperature for 30 s. DAPI antifade (10 μL) was infused into filters for 10 min to stain cell nuclei, and cells were imaged by fluorescence microscopy.

We also used single-cell off-chip FISH for analysis because of the difficulty of on-chip FISH due to bubble formation and high background. Male PBMCs were isolated by S-eDAR as above and their identities were confirmed by single-cell off-chip FISH to demonstrate a typical workflow. Here, sorted cells were collected in a multi-well plate and a single cell was picked up with a micromanipulator and placed onto a photo-etched coverslip with grids. The coverslip was dried and immersed in fixation buffer (3:1 methanol:acetic acid) for 1 h without agitation before FISH analysis.

3.3.6 Identification on fNRBCs by Immunostaining and FISH

fNRBCs from cord blood were selected as a model for verifying the enrichment performance

of the S-eDAR because of their low abundance in umbilical cord blood. Mononuclear cells were isolated from cord blood by density gradient centrifugation, labeled with PE-anti-CD71 antibody, and enriched by S-eDAR as described above. fNRBCs were alternatively isolated using the MiSelect R with the SelectChip Retrieval (MiCareo Inc., Taiwan). The collected cells were immunostained to confirm their identity as fNRBCs. Collected cells were fixed with 2% paraformaldehyde for 15 min, centrifuged, and washed twice. The cells were then permeabilized with 0.2% saponin and stained with Alexa Fluor 488 anti-CD45 antibody (10 μg/mL) for identification of WBCs, and with APC anti-HbF antibody (5 μg/mL) for identification of fNRBCs. DAPI (1 μg/mL) was used to stain cell nuclei. Cells were then washed, resuspended in Isoton II buffer, and transferred to a glass-bottom multi-well plate for imaging. For single-cell FISH analysis, fNRBCs (CD71+, HbF+, CD45-, DAPI+) were picked up with a micromanipulator and placed onto a photo-etched coverslip. The coverslip was dried and immersed in KCl solution (0.075 M, Sigma-Aldrich) for 30 min, then single-cell FISH was performed as described above and exhibited one red dot indicating the SRY gene on the Y chromosome, and one cyan dot indicating the X chromosome.

Isolating fNRBCs from concentrated adult female PBMCs. fNRBCs from cord blood were first confirmed as positive controls, then mononuclear cells from cord blood were mixed with PBMCs from healthy female donors, which were used as a mimic for fNRBCs in maternal PBMCs. The samples were labeled with PE-anti-CD71 antibody and were sorted by S-eDAR. Collected fNRBCs were identified by immunostaining and FISH analysis.

3.4 Results and Discussion

3.4.1 Workflow for Isolation and Confirmation of Rare Cells

The workflow for rare cell isolation by S-eDAR and characterization by immunostaining and FISH is shown in Figure 3.1. PBMCs were isolated from whole blood by density gradient centrifugation (Figure 3.1a), labeled with PE-tagged antibodies, and loaded onto an S-eDAR chip for sorting. The identity of the sorted cells was confirmed by immunostaining and by FISH (Figure 3.1b), an especially useful technique for noninvasive prenatal diagnosis.

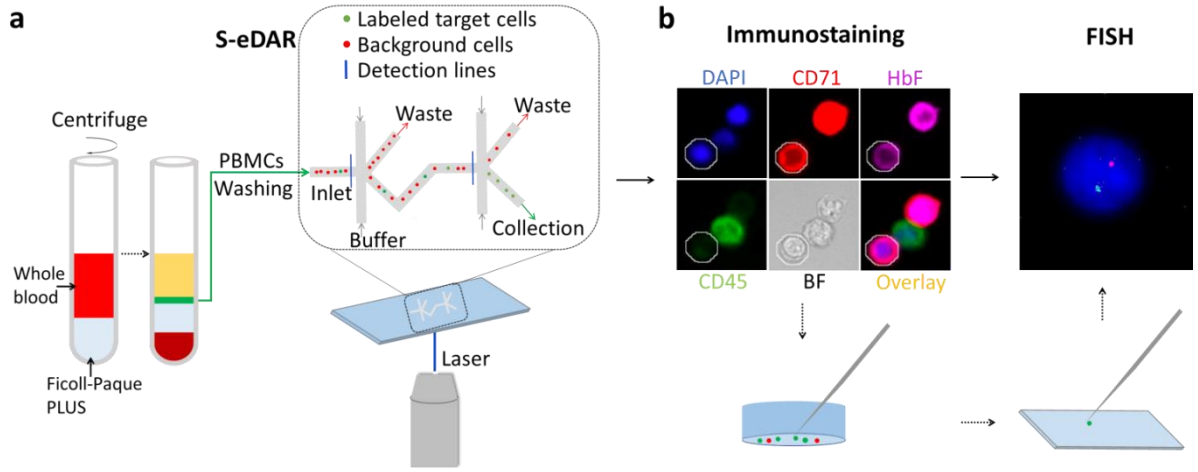

Figure 3.1 Workflow for isolation and confirmation of rare cells. (a) Diluted whole blood (red) was layered onto Ficoll-Paque PLUS (gray). After density gradient centrifugation, the thin middle layer (green) containing mononuclear cells between the plasma layer (yellow) and Ficoll-Paque PLUS layer (light blue) was removed and washed twice, then loaded onto a S-eDAR chip. Labeled target cells were sorted twice at two sorting junctions, accompanied by background cells. (b) The identities of the sorted cells were confirmed by immunostaining and FISH analysis. Once a target cell was confirmed by immunostaining, the cell was picked up by

a micromanipulator and transferred onto a slide for FISH analysis.

3.4.2 S-eDAR Performance on PBMCs and SNR

MCF-7 cells prelabeled with PE-anti-EpCAM antibody were spiked into concentrated PBMCs at different PBMC densities and cell sorting was performed using the S-eDAR system. Whole APD traces were recorded at two detection lines (Figure 3.2 a,b). The SNRs at the first and second detection lines were 64.0 and 87.2, respectively, for a sample with 2.5×10^7 PBMCs/mL; 37.0 and 51.7 for 5.0×10^7 PBMCs/mL; and 34.7 and 58.1 for 1.0×10^8 PBMCs/mL (Figure 3.2c). As PBMC density increased, SNR decreased but was still larger than 20, which was sufficiently sensitive for detection of MCF-7 cells[36], allowing a recovery rate of over 85% even at the highest PBMC density (Table 3.1).

Table 3.1 Recovery rate of spike-in MCF-7 cells from samples with different PBMC concentrations. In "L_S" samples, MCF-7 cells were first labeled with PE-anti-EpCAM antibody, then spiked into PBMCs. In the "S_L" sample, unlabeled MCF-7 cells were first spiked into a suspension of PBMCs, then labeled with PE-anti-EpCAM antibody.

PBMCs concentration (cells/mL)	2.5×10^7 (L_S)	5.0×10^7(L_S)	1.0×10^8(L_S)	2.5×10^7(S_L)
MCF-7 cells spiked	90	50	350	250
MCF-7 cells collected	80	43	299	218
Recovery rate	88.9%	86.0%	85.4%	87.2%

We also tested an alternate method in which unlabeled rather than prelabeled MCF-7 cells were spiked into PBMCs at 2.5×10^7 PBMCs/mL, and the sample was then labeled with

PE-anti-EpCAM antibody. With this method, the recovery rate was 87% and SNRs at the first and second detection lines were 38.7 and 55.4, respectively (Figure 3.2c). These SNRs were lower than when spiking prelabeled MCF-7 cells into 2.5×10^7 PBMCs/mL, likely due to free dyes in solution causing higher background.

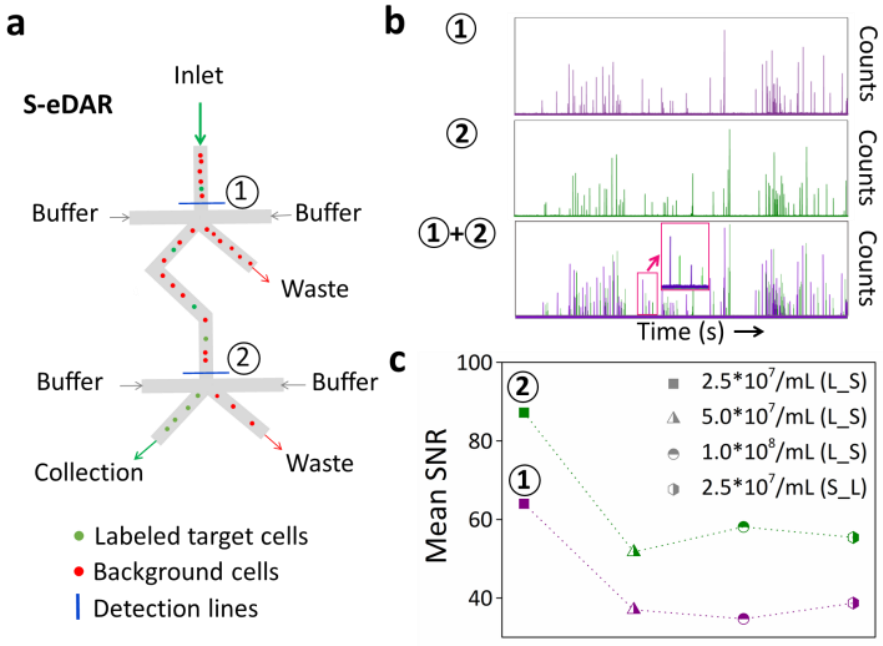

Figure 3.2 S-eDAR recovery rate and SNR. (a) Schematic showing how S-eDAR works. Labeled target cells are sorted at the two detection lines before collection. (b) Labeled MCF-7 cells were spiked into a suspension of PBMCs at 2.5×107 PBMCs/mL, then loaded onto a S-eDAR chip. APD traces at two detection lines and the overlay of two-channel traces were recorded. The inset in the overlay image shows that after a signal from a labeled cell was recorded at the first detection line (purple), a signal from the same labeled cell is subsequently detected at the second detection line (green). (c) The mean SNR was calculated for traces from experiments with different PBMC densities (2.5×107, 5.0×107, and 1.0×108 PBMCs/mL).

Since these three experiments used labeled MCF-7 cells spiked into PBMCs, they are referred to as 'L_S'. Experiments in which unlabeled MCF-7 cells were spiked into PBMCs at 2.5×107 PBMCs/mL and then labeled are referred to as 'S_L'.

3.4.3 On-chip Filters and FISH Analysis

FISH analysis was performed to confirm the identity of the male fNRBCs following isolation from concentrated PBMC samples by S-eDAR. As a model system, spike-in MCF-7 cells were used as the rare cells in initial experiments. On-chip filters with a 5-μm slit size were used first since such filters retain all sorted cells (Figure 3.3a). MCF-7 cells emitting strong PE signals stayed in filters and could be easily counted, and showed a high recovery rate (Figure 3.3 a,b).

PBMCs from healthy male and female donors were also used as model cells to develop the FISH analysis protocol. The sex chromosomes of these PBMCs were labeled with an SRY FISH probe after these cells were isolated by S-eDAR. Female PBMCs exhibited two fluorescent dots for the two X chromosomes, and male PBMCs showed one fluorescent dot. On-chip FISH was performed on female PBMCs following S-eDAR. With manually-triggered 'positive events', a small number of female PBMCs were sorted into filters where they were washed, fixed, dehydrated, denatured, and incubated overnight with SRY probes. One enriched cell is shown in a bright-field image in Figure 3.3c and in a fluorescence image in Figure 3.3d, showing the FISH results with two cyan dots indicating two X chromosomes.

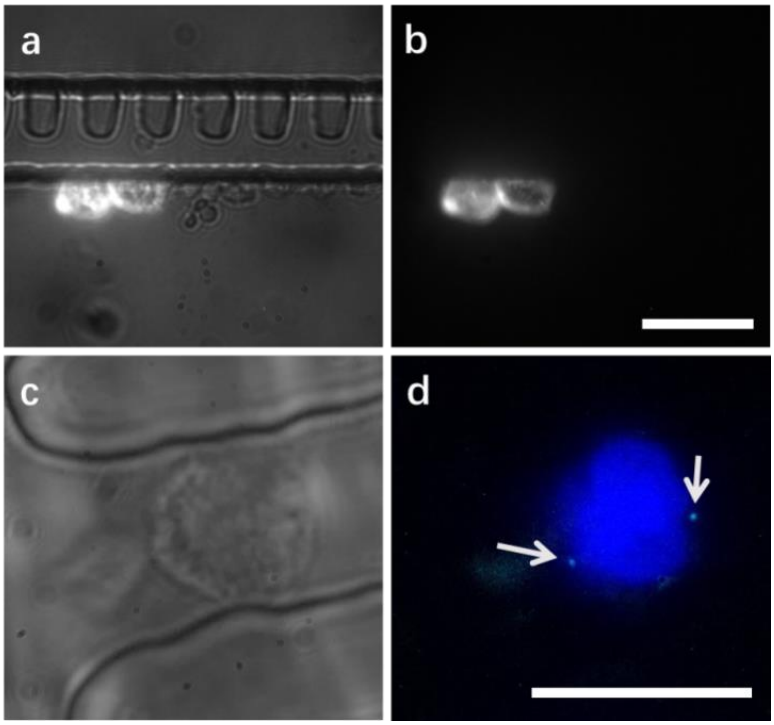

Figure 3.3 On-chip filters and FISH analysis. (a) Prelabeled MCF-7 cells were recovered by S-eDAR and remained in on-chip filters for enumeration by fluorescence microscopy. Overlay of fluorescence and bright-field images. b) Corresponding fluorescence image. Scale bar, 20 µm. (c) Female PBMC retained in an on-chip filter for reaction with SRY FISH probe. (d) Corresponding fluorescence image showing the cell nucleus labeled by DAPI (blue), and two X chromosomes visible as two small cyan dots on opposite sides of the nucleus. Scale bar, 10 µm.

Although on-chip filters allow a higher recovery rate, on-chip FISH posed several problems. First, micro-slits retained FISH probes, causing false-positive signals around cells. Second, bubbles entered the channels and caused high resistance, inhibiting subsequent infusion of buffer or reagents. Since we previously showed that off-chip collection with a multi-well plate can also achieve a high recovery rate (>85%), we used a micromanipulator to pick up

single cells from a multi-well plate (Figure 3.4a) and place them on a coverslip (Figure 3.4b) for single-cell FISH.

Single-cell FISH images showed one red dot indicating the SRY gene on the Y chromosome, and one cyan dot indicating the DXZ1 gene on the X chromosome (Figure 3.4c). To analyze the overall FISH success rate, five slides containing 261 total cells were tested. The success rate ranged from 64-80% for each slide (average, 71.6%) (Table 3.2). By adjusting the denaturation temperature to 78 °C, the overall success rate was improved to 85.7% (Table 3.3).

Table 3.2 Success rate of single-cell FISH analysis.

Slide No.	Counted cells	Cell with FISH signals	FISH success rate
1	100	80	80%
2	100	65	65%
3	25	16	64%
4	17	12	70.6%
5	19	14	73.7%
Total	261	187	71.6%

Table 3.3 The success rate of FISH analysis was improved by increasing the denaturation temperature.

Sample NO.	Temperature (℃)	FISH success rate
1	74	72.3%
2	76	80.0%
3	78	85.7%

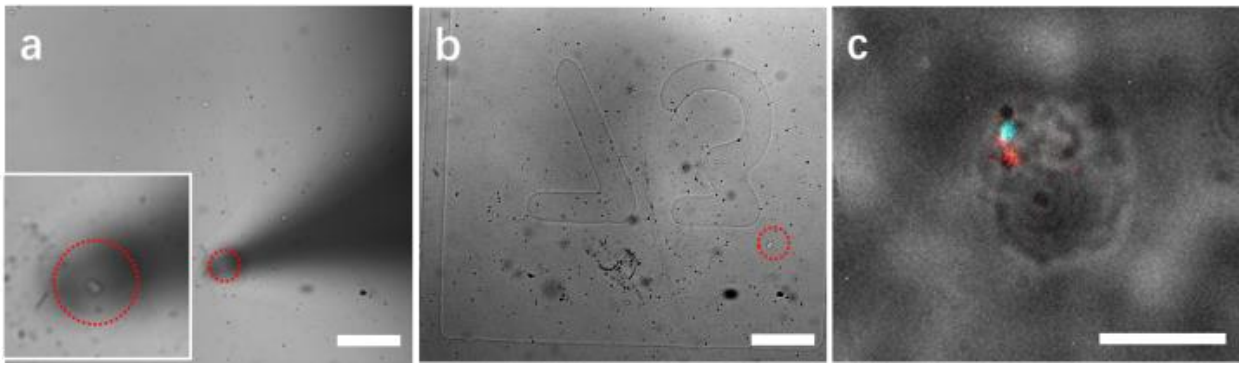

Figure 3.4 Single-cell FISH analysis. A single cell (inset) was picked up with a micromanipulator (a) and placed onto a coverslip with grids (b) for single-cell FISH analysis (c). Scale bars: 100 μm in (a) and (b); 10 μm in (c).

3.4.4 Isolation of fNRBCs from Adult Female PBMCs

We next applied S-eDAR to isolating male fNRBCs (from spike-in cord blood cells) from maternal PBMCs. As a positive control, we first isolated fNRBCs from cord blood, by first labeling cord blood with PE-anti-CD71 antibody, then sorting by S-eDAR, and immunostained with APC anti-HbF and Alexa Fluro 488 anti-CD45 antibodies (Figure 3.5a). SRY FISH probes were used to confirm the sorted fNRBCs. The fNRBCs (CD71+, HbF+, CD45-, DAPI+) were characterized by single-cell FISH, and exhibited one red dot indicating the SRY gene on the Y chromosome, and one cyan dot indicating the X chromosome.

Mononuclear cells from cord blood were then mixed with PBMCs from healthy adult female donors, which were used as a mimic for maternal PBMCs. The samples were labeled with PE-anti-CD71 antibody, enriched by S-eDAR, and immunostained. Immunostained fNRBCs were confirmed by FISH (Figure 3.5b). The positive SRY signal confirmed that fNRBCs

were of fetal origin since adult female cells have no SRY gene.

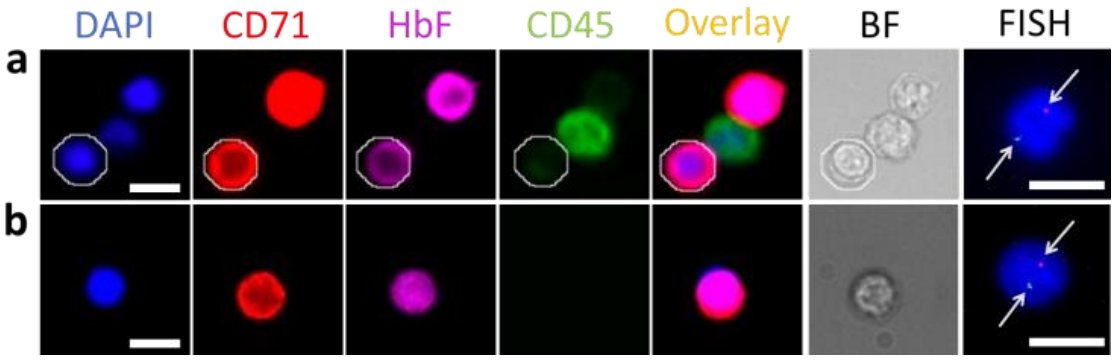

Figure 3.5 fNRBC isolation from maternal PBMCs. (a) fNRBCs from cord blood were labeled with PE-anti-CD71 antibody and sorted by S-eDAR. Enriched fNRBCs were identified by immunostaining with APC-anti-HbF and Alexa Fluor 488 anti-CD45 antibodies and with DAPI. fNRBCs were DAPI+, CD71+, HbF+, and CD45-, and white blood cells were DAPI+, CD71-, HbF-, and CD45+. One fNRBC is circled in white. In FISH analysis, male fNRBCs exhibited one red dot (arrow) indicating the SRY gene on the Y chromosome, and one cyan dot (arrow) indicating the X chromosome. (b) Mononuclear cells from cord blood were mixed with PBMCs from healthy adult female donors. fNRBCs were enriched by S-eDAR and identified by immunostaining and FISH analysis. Scale bar, 10 μm.

For control samples, there were no HbF+, CD71+, CD45-, DAPI+ cells found in PBMCs from healthy donor blood samples, indicating HbF is a specific marker towards labeling fNRBCs. Furthermore, we tested on 2nd trimester maternal blood with the same workflow, including running samples through S-eDAR and confirming fNRBCs with immunostaining. From 2nd trimester maternal blood, fNRBCs cells with HbF+, CD71+, CD45-, DAPI+ were

successfully enriched and confirmed with immunostaining, shown in Figure 3.6. Surrounding white blood cells were DAPI+, CD45+, HbF-, and CD71-.

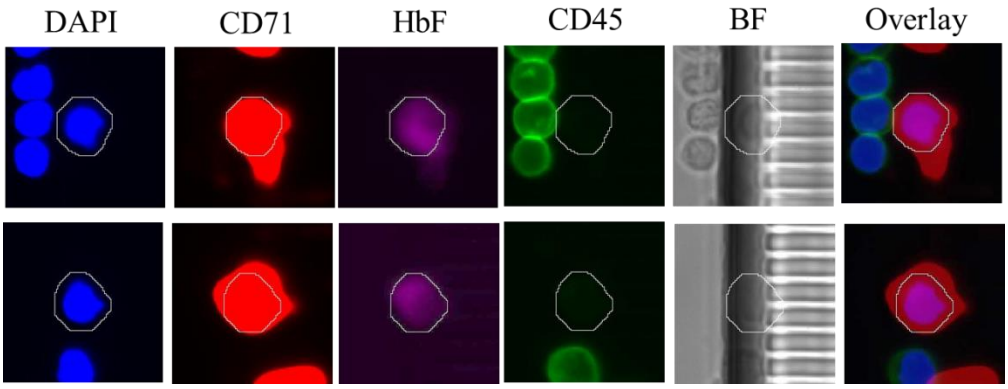

Figure 3.6 fNRBCs were found from 2nd trimester blood with DAPI+, CD71+, HbF+,CD45-. For PBMCs from healthy donor blood, there were no DAPI+, HbF+, C71+, CD45- cells ever found.

3.5 Conclusions

S-eDAR was used to recover rare cells spiked into concentrated PBMCs at 2-100×106 PBMCs/mL at a recovery rate of over 85% and a high SNR, similar to the performance of S-eDAR when using whole blood samples. However, by using concentrated PBMCs obtained by density gradient centrifugation rather than whole blood, the required sample volume was reduced and the antibody cost was reduced 20-fold. More importantly, this method enables a dramatic increase in the number of nucleated cells analyzed: processing 1 mL of PBMCs at the demonstrated 10^8/mL is equivalent to screening at least 20 mL of whole blood, since PBMCs yielded between 2 to 5 × 10^6 cells with density gradient separation from 1 mL whole blood, counted by using a hemocytometer. Rare cells isolated by S-eDAR remained viable for

downstream analysis by immunostaining and FISH. Isolated cells were collected either in an on-chip filter or in a multi-well plate from which individual cells were picked up with a micromanipulator for single-cell FISH. We also applied S-eDAR to sorting rare fNRBCs from cord blood and from cord blood cells spiked into concentrated adult female PBMCs, demonstrating the potential of S-eDAR for isolating rare fetal cells from maternal blood for noninvasive prenatal diagnosis. Furthermore, we were able to isolate fNRBCs from the 2nd trimester maternal PBMCs, showing the potential of utilizing this technology to enrich fetal cells for non-invasive prenatal diagnosis.

Chapter 4 Profiling Surfaces Protein on Individual Exosomes by a Single-Molecule Sensitive Flow Setup

4.1 Abstract

The single-molecule sensitive flow setup (SMSFS) combining microfluidics and fluorescence detection was validated with single molecules (PE-anti IgG and Alexa 647-anti IgG) at different concentrations. Then, surface protein markers of DiFi EVs (from DiFi human colorectal cancer cell line) including 3 classical exosomal markers (CD9, CD63 and CD81) and EGFR were characterized. Based the colocalization of fluorescence signals from protein markers and membrane dye, antibody-labeled exosomes can be clearly differentiated from free antibodies. The size information of exosomes can be characterized based on the fluorescence intensity from membrane dye-labeled exosomes.

4.2 Introduction

Exosomes are a subclass of membrane-coated extracellular vesicles with sizes of 40-160nm, containing biological cargo such as lipids, proteins, DNA, and RNA,[87] which are released from cells by exocytosis. Exosomes are found in most body fluids, and they have been shown to play key roles in processes such as coagulation, intercellular signaling, immune responses, and cellular waste management, [88] and the spread of cancer from primary tumor sites to metastasis sites. [89, 90] Exosomes are highly heterogeneous in molecular composition,[91, 92] and their surface proteins bear characteristics of their tissues of origin,[93] rendering specific

subclasses of these vesicles promising to demonstrate pathology affecting specific tissues.[94] They are promising biomarkers for liquid biopsy.[95, 96] The detailed information about surface proteins on exosomes, such as copy number, spatial distribution and interactions between various types of proteins is important to understand the role of exosomes. ELISA and western blot were often applied for bulk sample analysis, and they only provide information of average values. But some disadvantages exist, including requiring large amounts of samples, extensive post-labeling process for detection, low sensitivity and missing heterogeneity of individual exosomes. The small size and relatively low protein content of exosomes make them difficult to be characterized by conventional flow cytometry.[97] In recent years, novel technologies have been developed to increase the sensitivity of molecular profiling on exosomes, including multielectrode spectroscopy,[62] nano-plasmonic sensors,[60] nanopatterned microfluidic chips.[98, 99] Nano-plasmonic exosome sensors (nPLEX) utilize sophisticated nanohole arrays to first isolate single exosomes via specific capture antibodies, followed by protein profiling using detection antibodies.[60] Using nPLEX which had a great sensitivity to analyze ascites samples from ovarian cancer patients, and they found that exosomes derived from ovarian cancer cells can be identified by their expression of CD24 and EpCAM, suggesting the potential of exosomes as a biomarker for diagnostics.

More and more technology and platforms were developed to investigate the protein expression levels for exosome surface proteins, and some even focused on the heterogeneity of individual exosomes, including a proximity-dependent barcoding assay (PBA),[63] imaging[64]

and dedicated flow cytometry.[65] For PBA, a technique for analyzing surface proteins of individual exosomes, employing a combination of antibody-DNA conjugates and unique tag sequences repeated in large numbers of unique rolling circle amplification products for fluorescence detection was developed. By comparing the profiles of exosomes from different sources, specific surface protein combinations could be used for identification of exosomes that may be released to blood from specific tissues in health and disease. With imaging, multiplex protein markers on individual exosomes can be analyzed with multicolor labeling with different fluorophore-tagged antibodies. But the copy number of each marker has not been described in both works. Dedicated flow cytometry was optimized to characterize the copy number of surface protein on individual exosomes and their size information.[65] Since its detection sensitivity is not high to detect single molecules, it might miss small-size exosomes or exosomes with low copy number of markers. Even though some imaging techniques were developed to investigate the copy number of each marker on individual exosomes, e.g., quantitative single molecule localization microscopy (qSMLM)[100], but they usually have low throughput compared with flow-based techniques and they cannot sort exosome subpopulation for further analysis (e.g., PCR). Therefore, a novel platform is urgently needed to profile surface proteins in high multiplex and throughput for individual exosomes.

SMSFS is a sensitive fluorescence-based flow method that can achieve single molecule sensitivity with single molecules (e.g. PE/Alexa 647 labeled antibodies), which was developed for surface protein profiling on exosomes. In this work, the platform was applied

for detecting DiFi EVs, and the copy numbers for 5 markers, including CD9, CD63, CD81, TSMIX (mixture of CD9, CD63, CD81 tetraspanin markers) and EGFR, were characterized. SMSFS was based on a line-confocal design[101], including 4 lasers and 9 detectors. Difi EVs were stained with various antibody markers conjugated with different fluorophores and a membrane dye, ANEPPS. The transit time for each EV between multiple laser lines was characterized, and the flow rate in this laminar flow can be further calculated based on the linear velocity. The size distribution of Difi EVs was converted from fluorescence intensity measured with our home-built setup, since the fluorescence intensity is proportional to the surface area of the lipid membrane.[102, 103]

4.3 Experimental Section

4.3.1 Line Confocal Design Setup

A microfluidics setup based on a line confocal microscope was developed by our group recently.[102] The setup was built on an inverted microscope (Nikon TE2000). Four lasers, 405, 488, 561, and 640 nm, (100 mW, Coherent Obis) were used as excitation sources. The laser beams were focused onto a microfluidic chip using a 40× objective. Four laser lines were separated by 10 μm evenly. Fluorescence signals were filtered by bandpass filters, then through a 100 μm aperture, before being focused onto avalanche photodiodes APDs. The fluorescence filters for Di-8-ANEPPS, phycoerythrin (PE), and Alexa Fluor 647 were 600/50 nm, 609/34 nm, and 690/50 nm, respectively.

4.3.2 Microfluidic Channel Fabrication

Details of the microfabrication have been described previously.[101, 102] Using photolithography, the pattern on the photomask was transferred onto a silicon wafer. The wafer was silanized before using as a master to provide features to polydimethylsiloxane (PDMS). Reservoirs were created by punching holes on the two ends of the channels on PDMSs. At last, the PDMS was bonded to a clean coverslip after the treatment of oxygen plasma.

4.3.3 Single Molecules Tests

Single molecules, including alexa647 anti-IgG and PE anti-IgG (Biolegend) were tested in their corresponding detection channels. To differentiate signal from noise, a threshold was set as the average background plus 8/9 times the medium absolute deviation (MAD) of the data set. The intensity of each event was calculated as integration of the peak point and nearby 2 points after background subtraction. To calculate the recovery rate of single molecules, 10^8/ml of 200nm multicolor beads (final concentration when the sample was measured by the SMSFS) were added into single molecules to calculate the average flow rate. The laser power was 488nm, 10mw; 561nm, 10mw; 637nm, 100mw, when measuring alexa647 anti-IgG and PE anti-IgG molecules. 200nm multicolor beads were used to calibrate the setup, to guarantee optimal intensity and signal to noise ratio to be achieved when detecting these beads. Since 200nm beads have fluorescence signals in multiple channels, two different channels were selected, and then average delay time between these two channels can be resolved using the cross-correlation plot. Once the average delay time was resolved, the average linear velocity

and then flow rate can be calculated, ~15pL/s. The average concentration of single molecules was calculated based on the occurrence frequency of single molecules, and the average flow rate in each test. The recovery rate can be calculated as measured concentration/theoretical concentration of single molecules * 100%.

4.3.4 Labeling Protocol for DiFi EVs

DiFi EVs was isolated by sequential ultracentrifugation from the conditioned medium of DiFi cells, a human colorectal cancer cell line.[65] Human colorectal cancer (DiFi) cells were cultured in serum-free DMEM at 37 °C and 5% CO_2. DiFi-derived EVs were obtained by centrifuging a cell suspension for 10 min at 300 *g*, then centrifuging the supernatant for another 3000 *g* for 15 min with 0.22-mm polyether-sulfone filtration (Nalgene, Rochester, NY) to remove cellular debris and larger vesicles. The filtrate was concentrated with a 100k Centricon Plus-70 concentrator (Millipore, Germany) followed by ultracentrifugation at 165,000 *g* for 6 h to pellet EVs. Purified EVs were stored at 4 °C until further use.

Four Alexa647-tagged antibodies (ABs) were tested in this study, including CD9 (MEM61, Abcam), CD81 (FAB4615r, R&D), CD63 (H5C6, Biolegend), EGFR (EP38Y, Abcam), and four PE-tagged antibodies (ABs), including anti-human CD9 (HI9a, AAT Bioquest), anti-human CD81(5A6, Biolegend), anti-human CD63 (H5C6, Biolegend) and anti-human EGFR (AY13, Biolegend). The labeling protocol was shown below.

1. 1 μL EV(10^{12}/mL in PBS)+1 μL ABs, incubated for 1h (total volume is 2 μL).

2. Added 98 μL PBS buffer to dilute the sample and the final volume was 100 μL.

3. Added 1 μL of 20 μM ANEPPS (Thermo Fisher) in dimethyl sulfoxide to label lipid membranes for 1 h.

4. IZON columns were used to remove free antibodies.

5. For the IZON column, it was first washed the column with PBS buffer for 2 times (added 3mL of PBS for each time). Samples were diluted from 100 μl to 500 μL, and then added into the IZON column. After samples were completely flew through the column, 3mL of PBS buffer were added. At the end, 1mL of PBS buffer was added, and the sample was immediately collected once buffer was added.

6. Before flowing to SMSFS, 1 μL of 10% BSA was added to 99 μL samples to avoid nonspecific binding of EV onto the microfluidic channel. 10 μL of sample was loaded into the inlet reservoir of the microfluidic channel.

7. 488nm (10mw), 561nm (10mw) and 637nm (100mw) were used to excite ANEPPS, PE and Alexa-647 fluorophores, respectively. 5,000 to 10,000 events were collected to do the following data analysis.

4.3.5 Data Analysis

To differentiate signal from noise, a threshold was set as the average background plus 8/9 times of the medium absolute deviation of the background. Representative peaks were chosen by picking one point with higher intensity compared with nearby 4 points (2 left points and 2 right points). A filtering-bins (60 bins) was applied to remove the shoulder peak (comparing 2

adjacent peaks, if their time distance within 60 bins, keep the one with higher intensity). The transit time between two laser lines was determined by the cross-correlation analysis between the trajectories collected in the corresponding detection channels. The transit time was used to pick up colocalization events in different channels. Only when an antibody peak occurred within the expected time-window near a membrane dye peak, these peaks should come from an exosome. In these experiments, since exosomes were labeled with 2 color fluorophores, PE or Alexa Fluor 647-tagged antibody and a membrane dye, exosomes should be detected with a certain time delay in these two channels. Matlab built-in function xcorr(x,y) is used to analyze 2 channels' data and returns the cross-correlation plot of two discrete-time sequences, detected in corresponding channels. Cross-correlation measures the similarity between a vector x and shifted (lagged) copies of a vector y as a function of the lag (delay time). From the cross-correlation plot, the transit time in most frequency can be estimated.

An expected time-window was set as [-15 bins, +60 bins] for picking colocalization events (1 to 1 event-matching) with 2 channels data, which means only when an antibody peak occurred within the expected time-window (75 bins) near a membrane dye peak was the signal attributed to an exosome. Once all colocalized exosomes events were picked up, the exact transit time distribution was calculated based on the time point they occurred. The delay time in the cross-correlation plot and exact delay time distribution should match. If not, it indicates colocalization events with either large Anepps or antibody intensity events change the peak point location in the cross-correlation plot.

Non-colocalized antibody peaks were used to generate free antibody distributions. Once fluorescence signals from antibody markers on individual exosomes and free antibodies were characterized, copy number of exosomes can be resolved with 3 methods, deconvolution, median and mean copy number. Deconvolution analysis was performed as our group described previously.[102, 104] Median copy number was calculated as the median value of fluorescence intensity from antibody-labeled exosomes, divided by the median value of fluorescence intensity from free antibodies. Mean copy number was calculated as the mean value of fluorescence intensity from antibody-labeled exosomes, divided by the mean value of fluorescence intensity from free antibodies.

4.4 Results and Discussion

4.4.1 Single Molecules Tests

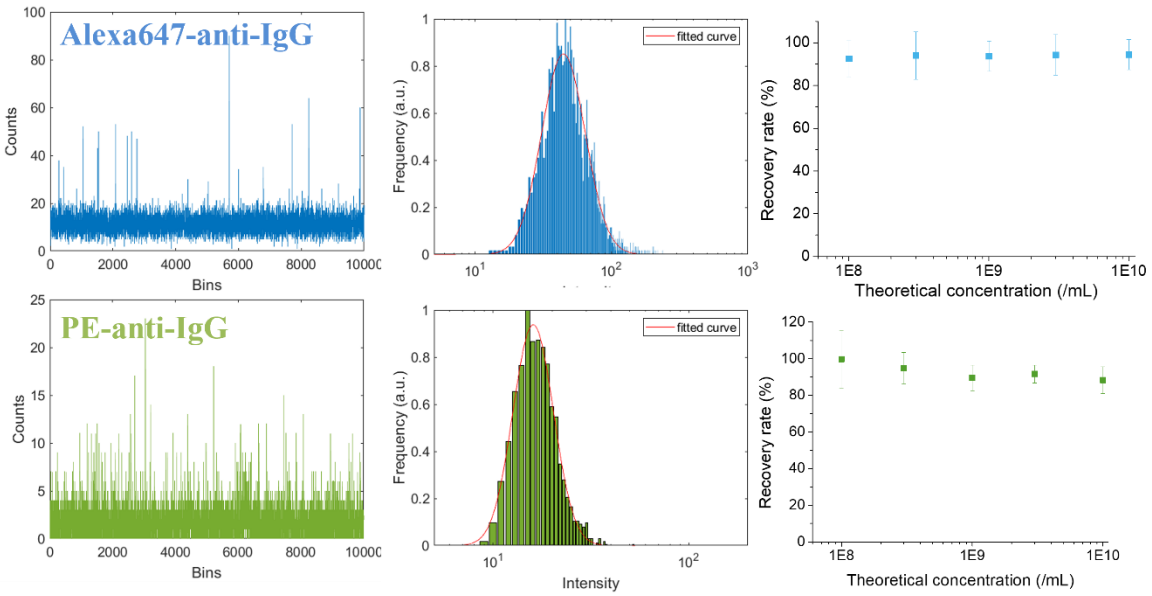

Figure 4.1 Data traces for Alexa647-anti-IgG and PE anti-IgG were recorded. Each

*representative peak indicates single molecule passing through the detection line. The intensity distribution of Alexa647-anti-IgG and PE anti-IgG can be fitted well with log-normal distribution (R^2>0.99). Recovery rates of Alexa647-anti-IgG and PE anti-IgG at different concentrations (10^8/mL, 3*10^8/mL, 10^9/mL, 3*10^9/mL and 10^{10}/mL) were measured.*

The Alexa Fluor 647 anti-IgG and PE anti-IgG were tested, showing representative peaks on data traces (Figure 4.1). The intensity distribution of alexa-647 anti-IgG and PE anti-IgG were shown, and the distribution can be fitted well with log-normal distribution.[104] The fluorescence intensity of single molecules depends on many factors, including single molecule emission kinetics, laser excitation profile across the detection line, photon collection efficiency varying spatially and flow profile, which contribute to the broad fluorescence intensity distribution of single molecules.

The recovery rate of single molecules, like alexa647-anti-IgG and PE-anti-IgG at 5 concentrations were tested. With multicolor beads, their fluorescent signals can be detected in least two channels. The average flow rate can be calculated once the average delay time was characterized from two channels' data. The recovery rate of single molecules can be calculated with the average flow rate and their measured frequency. The recovery rates for both molecules were more than 90%, indicating good sensitivity of the platform (Figure 4.1).

4.4.2 Colocalization, Cross-correlation and Delay Time Distribution for Exosomes

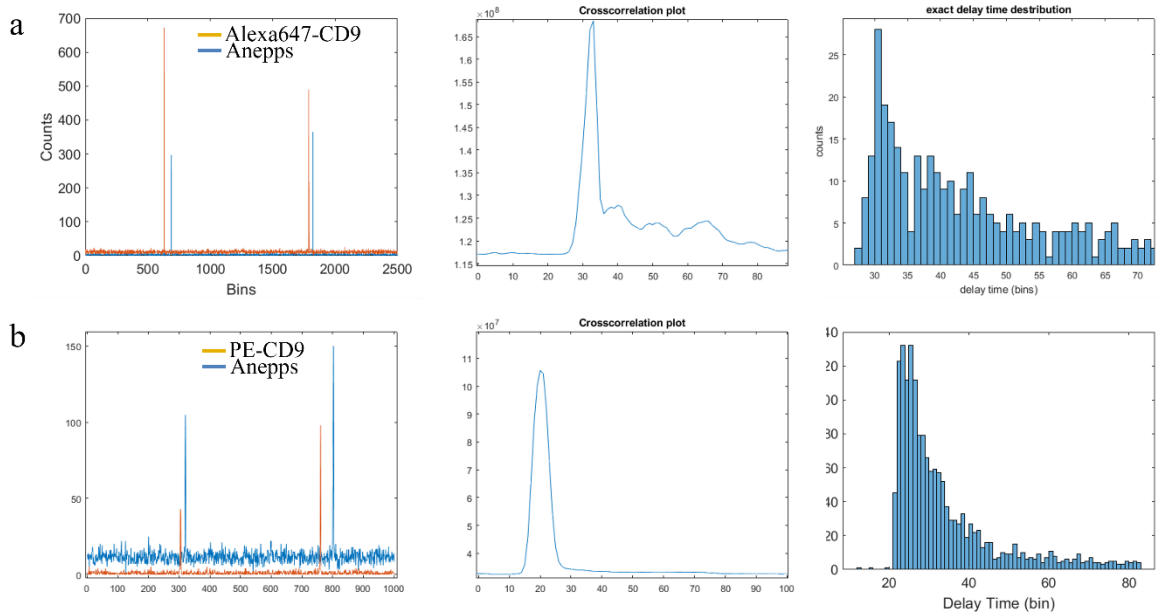

Figure 4.2 The overlay of data traces at 2 channels. Left: orange spikes indicate the occurrences of PE/Alexa647 events, and blue spikes indicates the occurrences of ANEPPS events. Middle: cross-correlation plots for 2 channels' data. Right: delay time distribution for colocalization events occurs in 2 channels.

Data traces for Difi EVs labeled with PE/Alexa 647-anti CD9 and Anepps were overlaid in Figure 4.2. Once events from two channels were close enough, less than 75 bins, they were regarded as colocalization events, indicating 1 exosome labeled with both PE/alexa647 and Anepps passed through 2 laser lines. The cross-correlation plot was analyzed with MATLAB scripts and the mode of delay time was estimated. Then a window for choosing colocalization events was set from mode of delay time minus 15 bins to mode of delay time plus 60 bins. Most of colocalization events from exosomes in these 2 channels can be picked up and the

delay time distribution can be characterized, so do the average flow rate and the concentration of antibody labeled exosomes.

4.4.3 Protein Profiling on DiFi EVs

Different concentrations of 4 markers (tagged with Alexa 647 and PE) were tested towards DiFi EVs to get the copy number at the saturated labeling conditions, shown in Figure 4.3 and 4.4. For Alexa 647 and PE labeled CD63, the error bar is larger, compared with other antibodies. One reason is due to low amounts of colocalization events from CD63-labeled exosomes. Another reason might be there are more heterogeneity for CD63 on DiFi EVs. Except for CD63, a much higher copy number was measured with Alexa647 tagged antibody than PE-tagged antibodies. There are 2 possible reasons, one is a crowding issue, because of the large size of a PE molecule, compared with a relatively small molecule, an Alexa 647 fluorophore. Another reason might be the bleed through of fluorescence signals from Anepps into PE detection channel causing ‘extra’ colocalization events with low fluorescence intensity in the PE channel, which would be regarded as exosomes with very low copy number. That would cause the total average copy number of PE labeled exosomes to be lower than that of Alexa 647 labeled exosomes. Similar as what flow cytometry does for compensation, A linear correction with fixed percentage, 6% (calibrated from Anepps only labeled DiFi EVs as a control sample), was used for compensation to remove the bleed through of Anepps signals into PE channel.

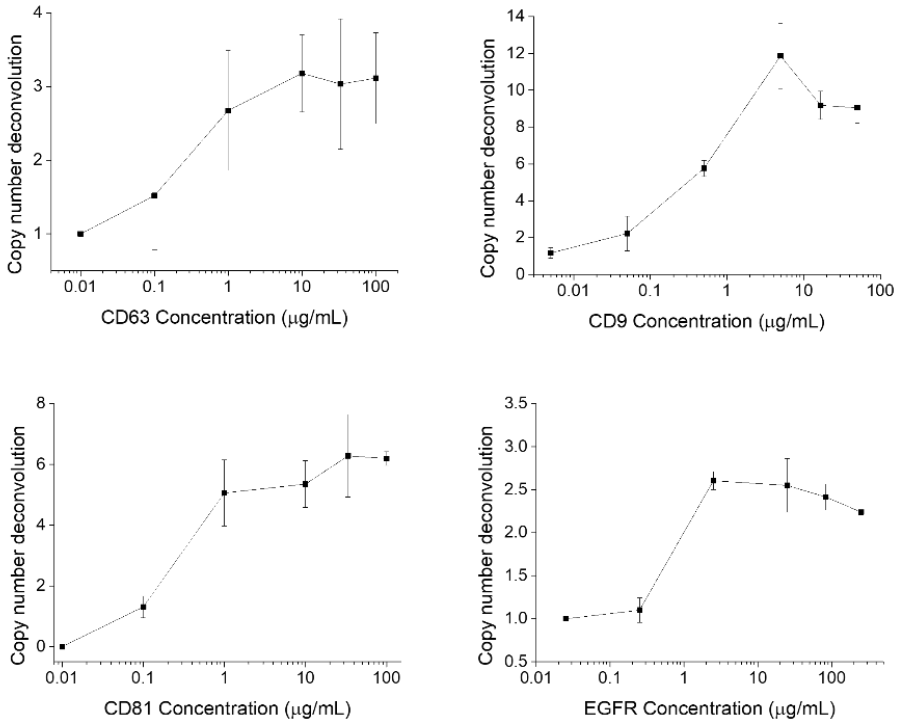

Figure 4.3 Titration analysis for 4 Alexa647-tagged protein markers. At the saturated labeling condition, the average copy number of alexa647-tagged CD63 (colocalization percentage: 20%), CD9 (50%), CD81 (50%) and EGFR (4%) for DiFi EVs were 3.2, 11.9, 6.3 and 2.6, respectively, determined from flow tests with deconvolution method.

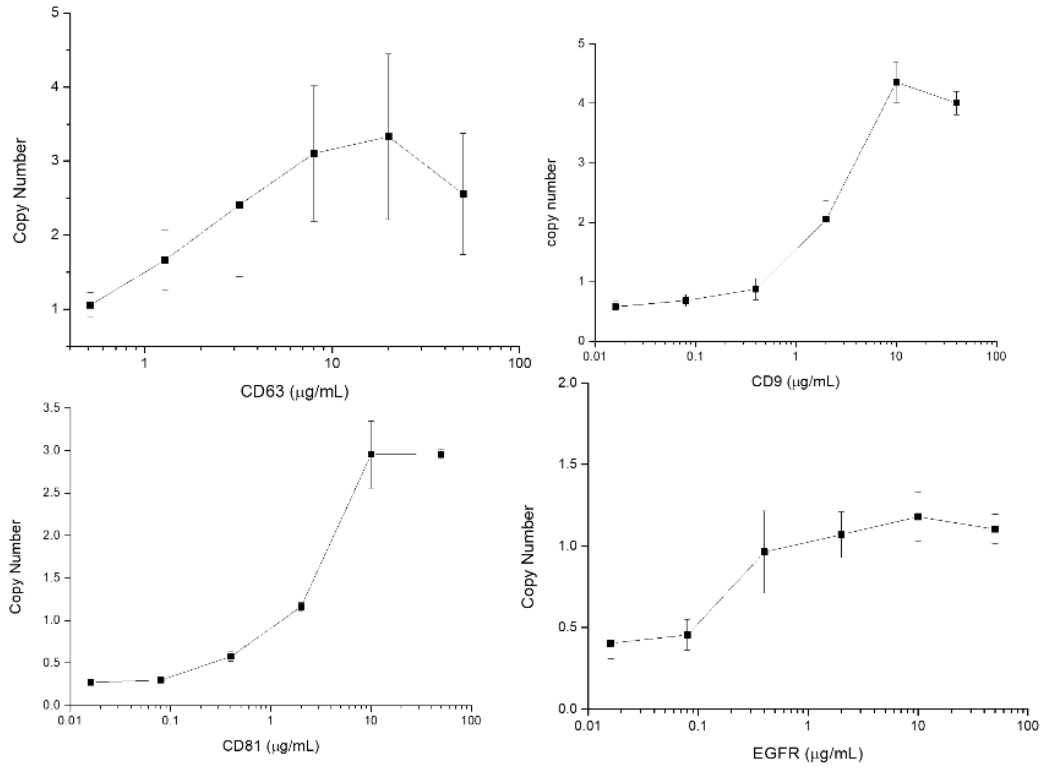

Figure 4.4 Titration analysis for 4 PE-tagged protein markers. At the saturated labeling condition, the average copy number of PE-tagged CD63 (colocalization percentage: 40%), CD9 (80%), CD81 (80%) and EGFR (26%) for DIFI EVs were 3.3, 4.4, 3.0 and 1.2, respectively.

4.4.4 PE Copy Number from SMSFS with 3 Methods

Samples labeled with 5 markers including CD9, CD81, CD63, TSMIX and EGFR at their saturated concentration were tested with SMSFS, and colocalization events were analyzed and the intensity distribution of individual exosomes in the PE channel were shown in Figure 4.5. The single PE intensity distribution in a yellow color was overlaid. With the

deconvolution method, their distributions of PE copy numbers were characterized, and the average copy numbers from deconvolution can be calculated. Compared with CD63 and EGFR, the distribution of PE copy number from CD9, CD81 and TSMIX was more symmetrical. On the contrary, there were more heterogeneity of CD63 and EGFR copy number on DiFi EVs.

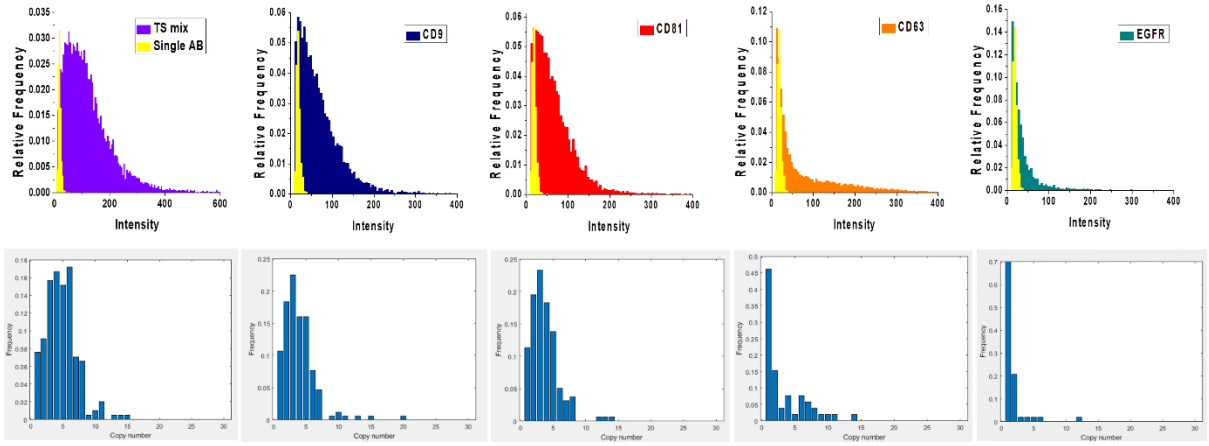

Figure 4.5 Fluorescent intensity histogram of DIFI EVs with five different markers and their copy numbers distribution. (TS mix, CD9, CD81, CD63 and EGFR), compared to intensity distribution of single antibodies, and their copy number distribution with deconvolution methods. The copy number calculated with deconvolution methods were 6.04, 3.56, 3.22, 3.96 and 1.95 for TS mix, CD9, CD81, CD63 and EGFR, respectively.

Their median and mean copy numbers were calculated for these 5 markers, shown in Figure 4.6. Comparing 3 methods for calculating the copy number, the median value of the copy numbers for CD63 and EGFR was much lower than the mean value and the average value from deconvolution. The reason was that for CD63 and EGFR, there were more

heterogeneity regarding to the number of antibodies labeled on the surface of exosomes. For the rest of markers, copy number values calculated with 3 methods were similar.

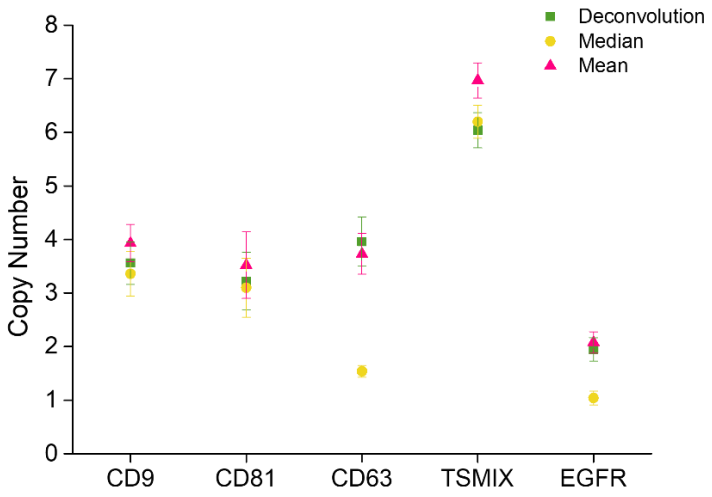

Figure 4.6 The copy number of 5 markers were calculated with 3 methods for comparison, including deconvolution, median and mean.

4.4.5 Correlating Anepps Intensity with Size of Individual Exosomes

Since the membrane dye intensity is linearly correlated with the area of exosomes, Stochastic Optical Reconstruction Microscopy (STORM) imaging was carried out to get the size distribution of individual exosomes as a reference (Figure 4.7 a). Furthermore, the size distribution from STORM imaging was correlated with fluorescence intensity from the membrane dye, measure with SMSFS, and a calibration curve to indicate the linear relationship between the fluorescence intensity and area of exosomes was plotted. With this

calibration curve, size of individual exosomes can be calculated, based on the membrane dye intensity. As a result, the size distribution with conversion from membrane dye intensity matched well with size distribution from STORM imaging. The copy number distribution and size distribution for PE labeled anti-CD9 exosomes were shown in figure 4.8.

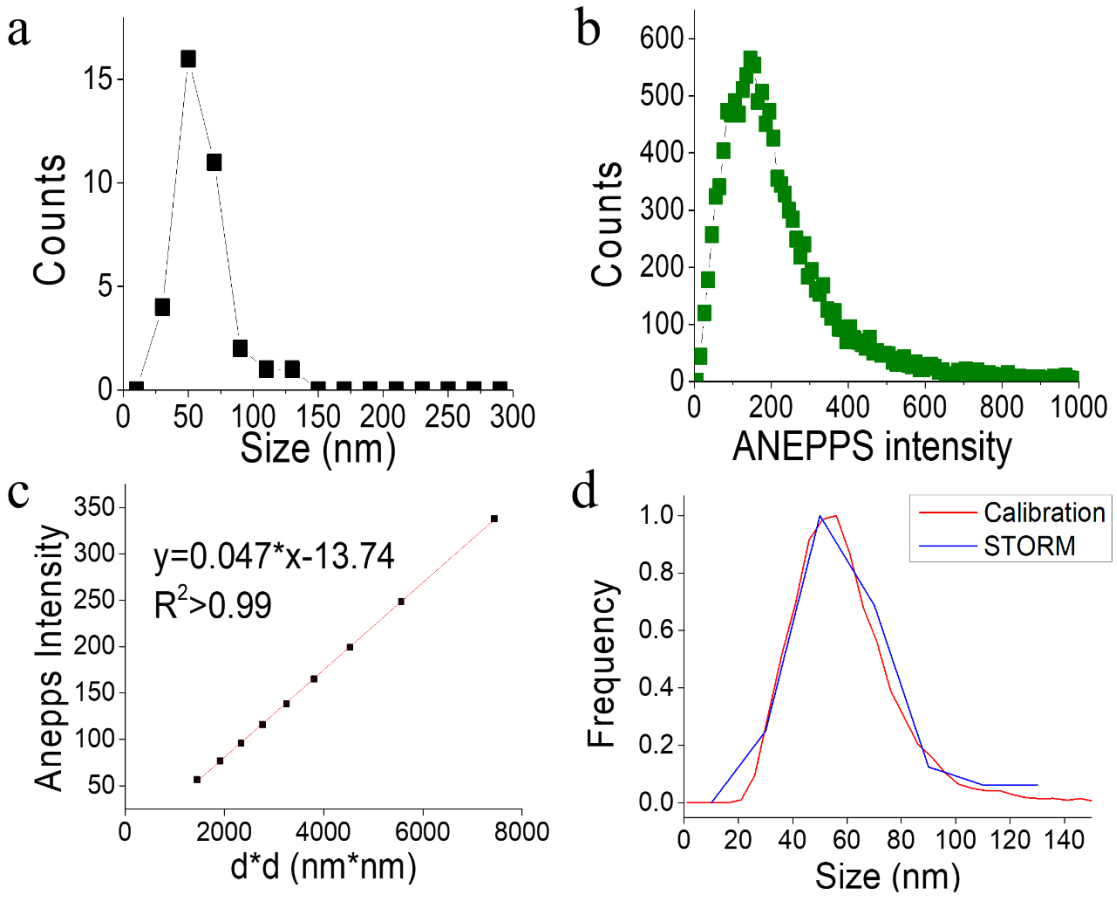

Figure 4.7 Correlating size information from STORM imaging with fluorescence intensity from the membrane dye. (a) size distribution for Anepps labeled DIFI EVs, measured by STORM imaging. (b) fluorescence intensity of Anepps intensity, measured by SMSFS. (c) the relation between Anepps intensity and d^2 was fitted with a linear calibration curve, $R^2 > 0.99$. (d) comparison between size distribution from STORM imaging and from conversion of Anepps

fluorescence intensity.

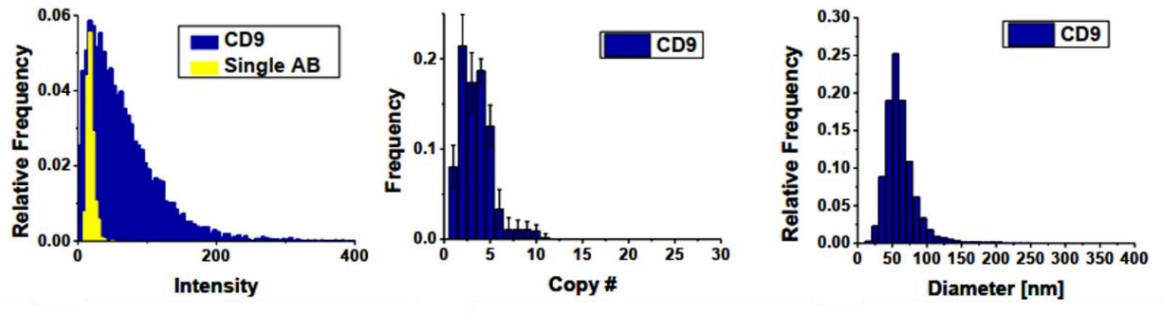

Figure 4.8 Copy number and size distribution of exosomes. Left: intensity distribution of CD9 labeled exosome (blue) and free CD9 antibody (yellow); Middle: copy number distribution of CD9+ exosomes with the deconvolution method; Right: size distribution of CD9+ exosomes, which was converted from membrane dye fluorescence intensity.

4.5 Conclusions

The flow platform (SMSFS) was first validated with Alexa 647 anti-IgG and PE anti-IgG molecules with good detection efficiency and high recovery rate (~90%), even for samples with low concentrations (e.g., 10^8/mL). Titration curves of 4 markers, including CD63, CD9, CD81 and EGFR were tested to find the saturated concentration of these markers on labeling DiFi EVs. The copy number of each marker on exosomes and their size distribution can be characterized.

In future work, the platform can characterize exosome subpopulations, and exosomes originated from various origins, like cancer, with plasma samples. It can characterize protein profiling for the early detection of cancer disease as a complementary analysis for CTCs. Except for cancer-related exosomes, exosomes related with pregnancy disorders, cardiovascular diseases, neurodegenerative diseases, and immune responses can be characterized.

Chapter 5 Conclusion and Perspective

This dissertation describes two platforms using microfluidic-based fluorescence detection for biomarker analysis. One platform was developed to enrich rare cells (e.g., circulating tumor cells and fetal nucleated red blood cells) with high purity and viability, which provided convenience for downstream analysis for single rare cells, including PCR, FISH, single cell sequencing, to obtain comprehensive molecular information about origin sites. In future, this platform can be applied readily to enrich other types of rare cells. Furthermore, the purity can be further enhanced by optimizing microfluidic designs.

The single molecule sensitive flow setup was applied to characterize copy number of protein markers on exosomes, but also indicating size information of exosomes. In future, this platform can be applied for differentiating EV subpopulations in plasma samples, similar like differentiating cell subpopulations with flow cytometry. Potential protein markers or marker combinations which can provide prognostic values for early detection of cancer, neurodegenerative, prenatal, and immune diseases, can be discovered with this robust platform.

References

1. Alimirzaie S, Bagherzadeh M, Akbari MR. Liquid biopsy in breast cancer: A comprehensive review. Clin Genet 2019;95(6):643-60.
2. Lin E, Cao T, Nagrath S, King MR. Circulating tumor cells: Diagnostic and therapeutic applications. Annu Rev Biomed Eng 2018;20:329-52.
3. Yu M, Stott S, Toner M, Maheswaran S, et al. Circulating tumor cells: approaches to isolation and characterization. J Cell Biol 2011;192(3):373-82.
4. Cristofanilli M, Budd GT, Ellis MJ, Stopeck A, et al. Circulating tumor cells, disease progression, and survival in metastatic breast cancer. N Engl J Med 2004;351(8):781-91.
5. Keller L, Pantel K. Unravelling tumour heterogeneity by single-cell profiling of circulating tumour cells. Nature Reviews Cancer 2019;19(10):553-67.
6. Plaks V, Koopman CD, Werb Z. Circulating tumor cells. Science 2013;341(6151):1186-8.
7. Zong C, Lu S, Chapman AR, Xie XS. Genome-wide detection of single-nucleotide and copy-number variations of a single human cell. Science 2012;338(6114):1622-6.
8. Pantel K, Alix-Panabières C. Real-time liquid biopsy in cancer patients: fact or fiction? Cancer Res 2013;73(21):6384-8.
9. Paterlini-Brechot P, Benali NL. Circulating tumor cells (CTC) detection: clinical impact and future directions. Cancer Lett 2007;253(2):180-204.
10. Dharmasiri U, Witek MA, Adams AA, Soper SA. Microsystems for the capture of low-abundance cells. Annual review of analytical chemistry 2010;3:409-31.
11. Alunni-Fabbroni M, Sandri MT. Circulating tumour cells in clinical practice: Methods of detection and possible characterization. Methods 2010;50(4):289-97.
12. Powell AA, Talasaz AH, Zhang H, Coram MA, et al. Single cell profiling of circulating tumor cells: transcriptional heterogeneity and diversity from breast cancer cell lines. PLoS One 2012;7(5):e33788.
13. Alix-Panabières C, Pantel K. Challenges in circulating tumour cell research. Nature Reviews Cancer 2014;14(9):623-31.
14. Zheng S, Lin H, Liu J-Q, Balic M, et al. Membrane microfilter device for selective capture, electrolysis and genomic analysis of human circulating tumor cells. J Chromatogr A 2007;1162(2):154-61.
15. Kahn HJ, Presta A, Yang L-Y, Blondal J, et al. Enumeration of circulating tumor cells in the blood of breast cancer patients after filtration enrichment: correlation with disease stage. Breast Cancer Res Treat 2004;86(3):237-47.
16. Kuo JS, Zhao Y, Schiro PG, Ng L, et al. Deformability considerations in filtration of biological cells. Lab on a Chip 2010;10(7):837-42.
17. Pinzani P, Salvadori B, Simi L, Bianchi S, et al. Isolation by size of epithelial tumor cells in peripheral blood of patients with breast cancer: correlation with real-time reverse

transcriptase–polymerase chain reaction results and feasibility of molecular analysis by laser microdissection. Hum Pathol 2006;37(6):711-8.
18. Lin HK, Zheng S, Williams AJ, Balic M, et al. Portable filter-based microdevice for detection and characterization of circulating tumor cells. Clinical Cancer Research 2010:1078-0432. CCR-10-1105.
19. Hou HW, Warkiani ME, Khoo BL, Li ZR, et al. Isolation and retrieval of circulating tumor cells using centrifugal forces. Sci Rep 2013;3:1259.
20. Coumans FA, van Dalum G, Beck M, Terstappen LW. Filter characteristics influencing circulating tumor cell enrichment from whole blood. PLoS One 2013;8(4):e61770.
21. Warkiani ME, Khoo BL, Wu L, Tay AKP, et al. Ultra-fast, label-free isolation of circulating tumor cells from blood using spiral microfluidics. Nat Protoc 2016;11(1):134.
22. Li M, Anand RK. High-throughput selective capture of single circulating tumor cells by dielectrophoresis at a wireless electrode array. J Am Chem Soc 2017;139(26):8950-9.
23. Allard WJ, Matera J, Miller MC, Repollet M, et al. Tumor cells circulate in the peripheral blood of all major carcinomas but not in healthy subjects or patients with nonmalignant diseases. Clin Cancer Res 2004;10(20):6897-904.
24. Riethdorf S, Müller V, Zhang L, Rau T, et al. Detection and HER2 expression of circulating tumor cells: prospective monitoring in breast cancer patients treated in the neoadjuvant GeparQuattro trial. Clin Cancer Res 2010:1078-0432. CCR-09-2042.
25. Xu H, Dong B, Xu S, Xu S, et al. High purity microfluidic sorting and in situ inactivation of circulating tumor cells based on multifunctional magnetic composites. Biomaterials 2017;138:69-79.
26. Balic M, Dandachi N, Hofmann G, Samonigg H, et al. Comparison of two methods for enumerating circulating tumor cells in carcinoma patients. Cytometry Part B: Clinical Cytometry: The Journal of the International Society for Analytical Cytology 2005;68(1):25-30.
27. Nagrath S, Sequist LV, Maheswaran S, Bell DW, et al. Isolation of rare circulating tumour cells in cancer patients by microchip technology. Nature 2007;450(7173):1235.
28. Dharmasiri U, Njoroge SK, Witek MA, Adebiyi MG, et al. High-throughput selection, enumeration, electrokinetic manipulation, and molecular profiling of low-abundance circulating tumor cells using a microfluidic system. Anal Chem 2011;83(6):2301-9.
29. Wang S, Liu K, Liu J, Yu ZTF, et al. Highly efficient capture of circulating tumor cells by using nanostructured silicon substrates with integrated chaotic micromixers. Angew Chem Int Ed 2011;123(13):3140-4.
30. Yu L, Ng SR, Xu Y, Dong H, et al. Advances of lab-on-a-chip in isolation, detection and post-processing of circulating tumour cells. Lab Chip 2013;13(16):3163-82.
31. Park M-H, Reátegui E, Li W, Tessier SN, et al. Enhanced isolation and release of circulating tumor cells using nanoparticle binding and ligand exchange in a microfluidic chip. J Am Chem Soc 2017;139(7):2741-9.
32. Stroock AD, Dertinger SK, Ajdari A, Mezić I, et al. Chaotic mixer for microchannels. Science 2002;295(5555):647-51.

33. Johnson ES, Anand RK, Chiu DT. Improved detection by ensemble-decision aliquot ranking of circulating tumor cells with low numbers of a targeted surface antigen. Anal Chem 2015;87(18):9389-95.
34. Yu M, Bardia A, Wittner BS, Stott SL, et al. Circulating breast tumor cells exhibit dynamic changes in epithelial and mesenchymal composition. Science 2013;339(6119):580-4.
35. Zhao M, Nelson WC, Wei B, Schiro PG, et al. New generation of ensemble-decision aliquot ranking based on simplified microfluidic components for large-capacity trapping of circulating tumor cells. Anal Chem 2013;85(20):9671-7.
36. Schiro PG, Zhao MX, Kuo JS, Koehler KM, et al. Sensitive and High-Throughput Isolation of Rare Cells from Peripheral Blood with Ensemble-Decision Aliquot Ranking. Angew Chem Int Ed 2012;51(19):4618-22.
37. Zhao M, Wei B, Nelson WC, Schiro PG, et al. Simultaneous and selective isolation of multiple subpopulations of rare cells from peripheral blood using ensemble-decision aliquot ranking (eDAR). Lab Chip 2015;15(16):3391-6.
38. Hou S, Chen JF, Song M, Zhu Y, et al. Imprinted NanoVelcro Microchips for Isolation and Characterization of Circulating Fetal Trophoblasts: Toward Noninvasive Prenatal Diagnostics. ACS Nano 2017;11(8):8167-77.
39. Bianchi DW, Zickwolf GK, Weil GJ, Sylvester S, et al. Male fetal progenitor cells persist in maternal blood for as long as 27 years postpartum. Proc Natl Acad Sci USA 1996;93(2):705-8.
40. Tjoa ML, Delli-Bovi L, Johnson KL, Bianchi DW. Antibodies to trophoblast antigens HLA-G, placenta growth factor, and neuroD2 do not improve detection of circulating trophoblast cells in maternal blood. Fetal Diagn Ther 2007;22(2):85-9.
41. Zhang L, Wang Y, Liao AH. Quantitative abnormalities of fetal trophoblast cells in maternal circulation in preeclampsia. Prenat Diagn 2008;28(12):1160-6.
42. Rezaei M, Winter M, Zander-Fox D, Whitehead C, et al. A reappraisal of circulating fetal cell noninvasive prenatal testing. Trends Biotechnol 2019;37(6):632-44.
43. Pertl B, Bianchi DW. First trimester prenatal diagnosis: Fetal cells in the maternal circulation. Semin Perinatol 1999;23(5):393-402.
44. Oudejans CBM, Tjoa ML, Westerman BA, Mulders MAM, et al. Circulating trophoblast in maternal blood. Prenat Diagn 2003;23(2):111-6.
45. Tilburgs T, Crespo ÂC, van der Zwan A, Rybalov B, et al. Human HLA-G+ extravillous trophoblasts: Immune-activating cells that interact with decidual leukocytes. Proc Natl Acad Sci USA 2015:201507977.
46. Sato Y, Fujiwara H, Zeng B-X, Higuchi T, et al. Platelet-derived soluble factors induce human extravillous trophoblast migration and differentiation: platelets are a possible regulator of trophoblast infiltration into maternal spiral arteries. Blood 2005;106(2):428-35.
47. Thomas DB, Yoffey J. Human foetal haemopoiesis I. The cellular composition of foetal blood. Br J Haematol 1962;8(3):290-5.
48. Millar D, Davis L, Rodeck C, Nicolaides K, et al. Normal blood cell values in the early

mid-trimester fetus. Prenat Diagn 1985;5(6):367-73.
49. Simpson JL, Elias S. Isolating fetal cells from maternal blood: advances in prenatal diagnosis through molecular technology. JAMA 1993;270(19):2357-61.
50. Wei X, Cai B, Chen K, Cheng L, et al. Enhanced isolation and release of fetal nucleated red blood cells using multifunctional nanoparticle-based microfluidic device for non-invasive prenatal diagnostics. Sensors Actuators B: Chem 2019;281:131-8.
51. Sun Y, Li N, Cai B, Wei X, et al. A Biocompatible Nanofibers-Based Microchip for Isolation and Nondestructive Release of Fetal Nucleated Red Blood Cells. Adv Mater Interfaces 2020:2001028.
52. Zheng Y, Carter NP, Price CM, Colman SM, et al. Prenatal diagnosis from maternal blood: simultaneous immunophenotyping and FISH of fetal nucleated erythrocytes isolated by negative magnetic cell sorting. J Med Genet 1993;30(12):1051-6.
53. Bianchi DW, Flint AF, Pizzimenti MF, Knoll J, et al. Isolation of fetal DNA from nucleated erythrocytes in maternal blood. Proc Natl Acad Sci USA 1990;87(9):3279-83.
54. He Z, Guo F, Feng C, Cai B, et al. Fetal nucleated red blood cell analysis for non-invasive prenatal diagnostics using a nanostructure microchip. J Mater Chem B 2017;5(2):226-35.
55. Wei X, Ao Z, Cheng L, He Z, et al. Highly sensitive and rapid isolation of fetal nucleated red blood cells with microbead-based selective sedimentation for non-invasive prenatal diagnostics. Nanotechnology 2018;29(43):434001.
56. Feng C, He Z, Cai B, Peng J, et al. Non-invasive Prenatal Diagnosis of Chromosomal Aneuploidies and Microdeletion Syndrome Using Fetal Nucleated Red Blood Cells Isolated by Nanostructure Microchips. Theranostics 2018;8(5):1301.
57. Cheng L, Wei X, Wang Z, Feng C, et al. Silica microbeads capture fetal nucleated red blood cells for noninvasive prenatal testing of fetal ABO genotype. Electrophoresis 2020;41(10-11):966-72.
58. Vossaert L, Wang Q, Salman R, Zhuo X, et al. Reliable detection of subchromosomal deletions and duplications using cell-based noninvasive prenatal testing. Prenat Diagn 2018;38(13):1069-78.
59. Van Niel G, d'Angelo G, Raposo G. Shedding light on the cell biology of extracellular vesicles. Nature reviews Molecular cell biology 2018;19(4):213-28.
60. Im H, Shao H, Park YI, Peterson VM, et al. Label-free detection and molecular profiling of exosomes with a nano-plasmonic sensor. Nat Biotechnol 2014;32(5):490-5.
61. Vlassov AV, Magdaleno S, Setterquist R, Conrad R. Exosomes: current knowledge of their composition, biological functions, and diagnostic and therapeutic potentials. Biochimica et Biophysica Acta (BBA)-General Subjects 2012;1820(7):940-8.
62. Kilic T, Cho YK, Jeong N, Shin I-S, et al. Multielectrode Spectroscopy Enables Rapid and Sensitive Molecular Profiling of Extracellular Vesicles. ACS Central Science 2022.
63. Wu D, Yan J, Shen X, Sun Y, et al. Profiling surface proteins on individual exosomes using a proximity barcoding assay. Nat Commun 2019;10(1):1-10.
64. Lee K, Fraser K, Ghaddar B, Yang K, et al. Multiplexed profiling of single extracellular

vesicles. ACS nano 2018;12(1):494-503.
65. Higginbotham JN, Zhang Q, Jeppesen DK, Scott AM, et al. Identification and characterization of EGF receptor in individual exosomes by fluorescence-activated vesicle sorting. Journal of Extracellular Vesicles 2016;5(1):29254.
66. Kuo JS, Zhao YX, Schiro PG, Ng LY, et al. Deformability considerations in filtration of biological cells. Lab Chip 2010;10(7):837-42.
67. Lin HK, Zheng S, Williams AJ, Balic M, et al. Portable filter-based microdevice for detection and characterization of circulating tumor cells. Clin Cancer Res 2010;16(20):5011-8.
68. Zhao M, Wei B, Chiu DT. Imaging multiple biomarkers in captured rare cells by sequential immunostaining and photobleaching. Methods 2013;64(2):108-13.
69. Driemel C, Kremling H, Schumacher S, Will D, et al. Context-dependent adaption of EpCAM expression in early systemic esophageal cancer. Oncogene 2014;33(41):4904.
70. Au SH, Edd J, Stoddard AE, Wong KH, et al. Microfluidic isolation of circulating tumor cell clusters by size and asymmetry. Sci Rep 2017;7(1):2433.
71. Williams MS, Longmuir KJ, Yager P. A practical guide to the staggered herringbone mixer. Lab Chip 2008;8(7):1121-9.
72. Chen Y, Li P, Huang P-H, Xie Y, et al. Rare cell isolation and analysis in microfluidics. Lab Chip 2014;14(4):626-45.
73. Racila E, Euhus D, Weiss AJ, Rao C, et al. Detection and characterization of carcinoma cells in the blood. Proc Natl Acad Sci USA 1998;95(8):4589-94.
74. Bankó P, Lee SY, Nagygyörgy V, Zrínyi M, et al. Technologies for circulating tumor cell separation from whole blood. J Hematol Oncol 2019;12(1):48.
75. Hyun K-A, Kwon K, Han H, Kim S-I, et al. Microfluidic flow fractionation device for label-free isolation of circulating tumor cells (CTCs) from breast cancer patients. Biosens Bioelectron 2013;40(1):206-12.
76. Tan SJ, Lakshmi RL, Chen P, Lim W-T, et al. Versatile label free biochip for the detection of circulating tumor cells from peripheral blood in cancer patients. Biosens Bioelectron 2010;26(4):1701-5.
77. Warkiani ME, Guan G, Luan KB, Lee WC, et al. Slanted spiral microfluidics for the ultra-fast, label-free isolation of circulating tumor cells. Lab Chip 2014;14(1):128-37.
78. Gertler R, Rosenberg R, Fuehrer K, Dahm M, et al. Detection of circulating tumor cells in blood using an optimized density gradient centrifugation. Molecular Staging of Cancer: Springer; 2003. p. 149-55.
79. Hur SC, Henderson-MacLennan NK, McCabe ER, Di Carlo D. Deformability-based cell classification and enrichment using inertial microfluidics. Lab Chip 2011;11(5):912-20.
80. Moon H-S, Kwon K, Kim S-I, Han H, et al. Continuous separation of breast cancer cells from blood samples using multi-orifice flow fractionation (MOFF) and dielectrophoresis (DEP). Lab Chip 2011;11(6):1118-25.
81. Huang S-B, Wu M-H, Lin Y-H, Hsieh C-H, et al. High-purity and label-free isolation of circulating tumor cells (CTCs) in a microfluidic platform by using

optically-induced-dielectrophoretic (ODEP) force. Lab Chip 2013;13(7):1371-83.
82. Cima I, Wen Yee C, Iliescu FS, Min Phyo W, et al. Label-free isolation of circulating tumor cells in microfluidic devices: Current research and perspectives. Biomicrofluidics 2013;7(1):011810.
83. Johnson ES, Xu S, Yu H-M, Fang W-F, et al. Isolating Rare Cells and Circulating Tumor Cells with High Purity by Sequential eDAR. Anal Chem 2019;91(22):14605-10.
84. Bianchi DW, Zickwolf GK, Yih MC, Flint AF, et al. Erythroid-specific antibodies enhance detection of fetal nucleated erythrocytes in maternal blood. Prenat Diagn 1993;13(4):293-300.
85. Sohda S, Arinami T, Hamada H, Nakauchi H, et al. The Proportion of Fetal Nucleated Red Blood Cells in Maternal Blood: Stimation by FACS Analysis. Prenat Diagn 1997;17(8):743-52.
86. Qin Y, Wu L, Schneider T, Yen GS, et al. A Self-Digitization Dielectrophoretic (SD-DEP) Chip for High-Efficiency Single-Cell Capture, On-Demand Compartmentalization, and Downstream Nucleic Acid Analysis. Angew Chem Int Ed 2018;130(35):11548-53.
87. Théry C, Zitvogel L, Amigorena S. Exosomes: composition, biogenesis and function. Nature reviews immunology 2002;2(8):569-79.
88. Andaloussi SE, Mäger I, Breakefield XO, Wood MJ. Extracellular vesicles: biology and emerging therapeutic opportunities. Nature reviews Drug discovery 2013;12(5):347-57.
89. Hoshino A, Costa-Silva B, Shen T-L, Rodrigues G, et al. Tumour exosome integrins determine organotropic metastasis. Nature 2015;527(7578):329-35.
90. Costa-Silva B, Aiello NM, Ocean AJ, Singh S, et al. Pancreatic cancer exosomes initiate pre-metastatic niche formation in the liver. Nat Cell Biol 2015;17(6):816-26.
91. Poliakov A, Spilman M, Dokland T, Amling CL, et al. Structural heterogeneity and protein composition of exosome-like vesicles (prostasomes) in human semen. The Prostate 2009;69(2):159-67.
92. Yuana Y, Koning RI, Kuil ME, Rensen PC, et al. Cryo-electron microscopy of extracellular vesicles in fresh plasma. Journal of extracellular vesicles 2013;2(1):21494.
93. Larssen P, Wik L, Czarnewski P, Eldh M, et al. Tracing cellular origin of human exosomes using multiplex proximity extension assays. Mol Cell Proteomics 2017;16(3):502-11.
94. Peinado H, Alečković M, Lavotshkin S, Matei I, et al. Melanoma exosomes educate bone marrow progenitor cells toward a pro-metastatic phenotype through MET. Nat Med 2012;18(6):883-91.
95. Santiago-Dieppa DR, Steinberg J, Gonda D, Cheung VJ, et al. Extracellular vesicles as a platform for ‘liquid biopsy’in glioblastoma patients. Expert review of molecular diagnostics 2014;14(7):819-25.
96. Yoshioka Y, Kosaka N, Konishi Y, Ohta H, et al. Ultra-sensitive liquid biopsy of circulating extracellular vesicles using ExoScreen. Nat Commun 2014;5(1):1-8.
97. Van der Pol E, Coumans F, Grootemaat A, Gardiner C, et al. Particle size distribution of exosomes and microvesicles determined by transmission electron microscopy, flow

cytometry, nanoparticle tracking analysis, and resistive pulse sensing. J Thromb Haemost 2014;12(7):1182-92.
98. Zhang P, Wu X, Gardashova G, Yang Y, et al. Molecular and functional extracellular vesicle analysis using nanopatterned microchips monitors tumor progression and metastasis. Sci Transl Med 2020;12(547):eaaz2878.
99. Zhang P, Zhou X, He M, Shang Y, et al. Ultrasensitive detection of circulating exosomes with a 3D-nanopatterned microfluidic chip. Nature biomedical engineering 2019;3(6):438-51.
100. Lennon KM, Wakefield DL, Maddox AL, Brehove MS, et al. Single molecule characterization of individual extracellular vesicles from pancreatic cancer. Journal of extracellular vesicles 2019;8(1):1685634.
101. Schiro PG, Kuyper CL, Chiu DT. Continuous-flow single-molecule CE with high detection efficiency. Electrophoresis 2007;28(14):2430-8.
102. Jiang Y, Andronico LA, Jung S-R, Chen H, et al. High-Throughput Counting and Superresolution Mapping of Tetraspanins on Exosomes using a Single-Molecule Sensitive Flow Technique and Transistor-like Semiconducting Polymer Dots. Angew Chem Int Ed 2021.
103. Andronico LA, Jiang Y, Jung S-R, Fujimoto BS, et al. Sizing Extracellular Vesicles Using Membrane Dyes and a Single Molecule-Sensitive Flow Analyzer. Anal Chem 2021;93(14):5897-905.
104. Mutch SA, Fujimoto BS, Kuyper CL, Kuo JS, et al. Deconvolving single-molecule intensity distributions for quantitative microscopy measurements. Biophys J 2007;92(8):2926-43.